Capacity of Multiple-Input Multiple-Output Wireless Communication Systems Operating in the HF Band

by

Nigel Leonard Brine

B E (Computer Systems Engineering)

Thesis submitted for the degree of

Doctor of Philosophy

in

School of Electrical and Electronic Engineering,
Faculty of Engineering,
Computer and Mathematical Sciences

The University of Adelaide, Australia

2010

Chapter 1

Introduction

Spatial multiplexing is a wireless communication technique that employs MIMO (multiple-input multiple-output) antenna arrays and spatial signal processing to effectively establish multiple parallel spatial data pipes within the same frequency band, leading to large capacity gains [1], [2], [3], [4], [5]. The capacity that can be achieved using this technique is dependent on a number of factors, one of the most significant of these being multipath richness in the communication channel. In general, an increase in multipath richness will lead to an increase in the number of parallel spatial data pipes that can be supported, leading to higher capacities. The transfer function of the MIMO communication channel is a matrix of the complex transfer functions between each transmit and receive antenna pair. The number of parallel spatial data pipes that can be supported by the channel is given by the *rank* of the channel matrix [6].

Most MIMO wireless communications research has targeted indoor and short-range outdoor environments at frequencies of the order of 1 to 5 GHz [5], [7], [8], [9], [10]. For such scenarios, the bandwidth available is large, antennas are small, cheap to produce, and may be closely spaced, and the channel is typically rich in scattering, leading to high rank channel matrices which offer large capacities. Key applications for this research includes wireless LAN (local area network) (IEEE 802.11n) [11], [12], [13], [14], [15] and personal communication devices [16], [17], [18], [19], [20].

The HF (high frequency) band is subject to significant multipath caused by multiple refractions and reflections between the ionospheric layers and the earth's surface. While multipath fading limits the capacity offered by traditional SISO (single-input single-output) techniques, it makes the HF band a potential candidate for MIMO techniques. A major application that

stands to benefit from HF MIMO technology is ship-based communications. The Australian Navy, for example, currently uses SISO HF radios as backups to the satellite communications systems in place for delivering high data rates to ships at sea. The backup radios are unable to support the data rates typically required, while satellite systems are costly to implement and maintain. An HF system employing spatial multiplexing may prove to be a suitable alternative. To the best of our knowledge, no prior investigation has been made into the performance of spatial multiplexing in the HF band. Note that just prior to the submission of this thesis, additional research into HF MIMO communications started to appear [21], [22], [23], [24], [25], [26].

The capacity of MIMO wireless communication systems operating in the HF band is the topic of this thesis. By estimating HF MIMO capacity, the suitability of MIMO techniques for the HF band can be determined. Factors that are likely to limit capacity and affect the design of HF MIMO systems, such as the number of propagating modes, and propagating mode and antenna correlation, are also of interest. Problems to address include establishing a model for the HF MIMO channel, devising a technique for estimating HF MIMO capacity, and developing a system for the collection of multi-channel HF radio data, while keeping cost, schedule and risk under control.

1.1 Measuring of MIMO Capacity Through Direct Recording of Channel Matrices

A typical approach to measuring MIMO capacity involves using transmit and receive antenna arrays to record channel matrices directly, which are then substituted into the general MIMO capacity equation so that capacity can be calculated [9]. For the HF scenario, recording channel matrices directly has a number of problems. The approach is subject to logistical issues, since recording HF MIMO channel matrices requires transmit and receive systems to be operated up to hundreds or thousands of kilometres apart. The approach is also subject to significant development cost, time and risk, since recording HF MIMO channel matrices requires design and implementation of multi-channel transmit and receive systems with a large number of elements. In addition, the number of transmit and receive elements to use is not known. The maximum rank of the recorded channel matrices is limited by the number of transmit and receive elements used, so the number of transmit and receive elements used should be greater than the number of parallel spatial data pipes, or eigenmodes, of the underlying channel. Ideally an

approach to measuring HF MIMO capacity should be sought which minimises the number of transmit and receive elements required, and does not impose an upper limit on channel matrix rank. Furthermore, recording channel matrices directly involves considering a fixed frequency only, however the HF band covers a wide range of frequencies (typically 3 - 30 MHz), and the channel properties vary wildly across the band. A more suitable approach is to perform a sweep of the complete HF band, such that capacity can be calculated at each frequency in the band, allowing the maximum capacity available in the band to be determined.

1.2 A Technique for Estimating HF MIMO Capacity

A technique for estimating HF MIMO capacity has been devised which addresses the problems identified with direct recording of channel matrices. The technique involves recording oblique FMCW (frequency modulated continous wave) HF sounder data [1] using a single transmit antenna element, and a small number of receive antenna elements. The recorded HF sounder data is processed to obtain antenna correlation and mode correlation matrices. MIMO channel matrices are generated from the antenna and mode correlation matrices, and subsituted into the general MIMO capacity equation to obtain capacity.

The technique has a number of advantages. Only a small number of receive elements are required, along with a single transmit element. The single transmit element can be any existing ionosonde transmitter on a GPS (global positioning system) locked time schedule. Thus we only need be concerned with the design, implementation and operation of the receiver, avoiding the logistical issues associated with long distance HF measurements. FMCW HF data is recorded, allowing the entire HF band of frequencies to be analysed. The maximum capacity available at a given point in time can therefore be estimated. The multipath structure of the channel is considered, and the underlying channel eigenmodes are revealed, allowing a suitable size for MIMO transmit and receive arrays to be determined. The rank of the generated channel matrices is not limited by the number of antenna elements used to record the data, but instead by the amount of multipath or number of *propagating modes*, correlation between propagating modes, and correlation between antenna elements. The devised technique can also be extended to measure time correlation of the channel. Channel matrix estimates are typically made at the receive end of MIMO systems, and used in the spatial processing algorithm to recover the

[1] FMCW HF sounders are also referred to as *ionosondes*

transmit signal vector. Time correlation measurements can be used to determine an appropriate interval between channel matrix estimates.

1.3 Approach Taken in Investigating HF MIMO Capacity

The following subsections describe the approach taken in investigating HF MIMO Capacity.

1.3.1 Background Theory and Literature Survey

The first step involved studying capacity, MIMO capacity, and the HF channel. Important background theory for these topics is presented in Chapter 2, while a survey of relevant research literature is presented in Chapter 3.

1.3.2 Initial Estimate of HF MIMO Capacity

The technique devised for estimating HF MIMO capacity relies on the recording of oblique ionosonde data with a small number of receive antenna elements. In order to record this data, an MCR (multi-channel receiver) had to be designed, constructed and operated. Due to the level of effort required to develop the MCR, an initial investigation was first performed that involved analysis of an existing set of HF sounder data. The set of HF sounder data analysed was collected by the DSTO (Defence Science and Technology Organisation) from its LLISP (Low Latitude Ionospheric Sounding Project) network of oblique ionosondes, and stored as ionogram images. These ionograms were not suitable for an in depth analysis of HF MIMO capacity, but allowed an initial estimate of capacity to be made. The details of this initial capacity estimate are provided in Chapter 4. The positive results obtained indicated that spatial multiplexing was a promising HF communications technique worthy of further investigation.

1.3.3 MCR Development

Following the initial estimate of HF MIMO Capacity, development of the MCR commenced. The MCR was developed from scratch due to no commercially available products adequately meeting our set of requirements, which included direct digital sampling, high dynamic range,

high decimation rate, local oscillator sweep capability, local oscillator synchronisation to GPS, four receiver channels, and the ability to tune the four receiver channels to two different frequencies simultaneously. This last requirement was important for performing noise and interference measurements, and also allowed for time correlation measurements to be performed. The main tasks involved with MCR development included requirements analysis, system modelling, FPGA (field programmable gate array) hardware utilisation estimates, trade studies, board schematic design, DDC (digital down converter) chip design, FPGA firmware design, board testing and debugging, console and data logging software design, and system testing and debugging. MCR development is described in detail in Appendix A.

1.3.4 Data Collection

Upon completion of testing and debugging, the MCR was set up at DSTO with existing receiving infrastructure comprising antenna arrays, and an automatic gain control system. The MCR was configured to track signals from two ionosonde transmitters located in Darwin over a 48 hour period. For the first half of this period a spatial antenna array was used, while for the second half a cross-polarized antenna array was used. Received data was saved to a hard drive for later analysis. Details of the data collection process are provided in Chapter 6.

1.3.5 Post-Processing of HF Sounder Data

The post-processing applied to the received data included sweep difference correction, and additional decimation filtering. Ionograms were generated by performing an FFT (fast Fourier transform) on small blocks of the post-processed receive data. Details regarding post-processing and ionogram generation, along with relevant ionogram equations, are provided in Chapter 6.

1.3.6 HF MIMO Channel Matrix Model

Analysis of the generated ionograms lead to the development of a model for the structure of the HF MIMO channel matrix. The model indicates that, for the case where the elements of the transmit and receive arrays are closely spaced, the rank of the HF MIMO channel matrix is a function of the number of transmit and receive antenna elements, transmit and receive antenna

correlation, the number of propagating modes, and propagating mode correlation. Details of the HF MIMO channel matrix model are provided in Chapter 5.

1.3.7 Gesbert Channel Matrix Equation

The Gesbert channel matrix equation [27] can be used to generate stochastic channel matrices from receive antenna correlation, mode correlation, and transmit antenna correlation matrices. The rank properties of channel matrices generated by this equation match the rank properties of the HF MIMO channel matrix model. Because MIMO capacity is a function of channel matrix rank, it is reasonable to estimate capacity by measuring the receive antenna correlation, propagating mode correlation, and transmit antenna correlation matrices, substituting the receive antenna correlation, propagating mode correlation, and transmit antenna correlation matrices into the Gesbert channel matrix equation to yield a stochastic channel matrix, and substituting the generated stochastic channel matrix into the general MIMO capacity equation, to yield the HF MIMO capacity estimate. An analysis of the Gesbert channel matrix equation is provided in Chapter 5.

1.3.8 Antenna and Mode Correlation Calculations

Techniques for calculating antenna and mode correlation from ionograms were devised and applied to the ionograms obtained using the MCR, such that antenna and mode correlation matrices could be generated. Details of these techniques, along with the results obtained, are provided in Chapter 7.

1.3.9 HF MIMO Capacity Calculations

The resulting antenna and mode correlation matrices were substituted into the Gesbert channel matrix equation to obtain stochastic channel matrices. The stochastic channel matrices were substituted into the general MIMO capacity equation to yield HF MIMO capacity estimates. HF MIMO capacity was also calculated with correlation matrices set to the identity matrix, which represents full decorrelation, and the all ones matrix, which represents full correlation. This allowed the effect of correlation on capacity to be investigated. Details of the HF MIMO capacity calculation procedure, along with the results obtained, are provided in Chapter 8.

1.3.10 Identification of Future Research Directions

A number of important areas for future HF MIMO capacity research have been identified, and these are discussed in Chapter 9.

1.4 Contributions Made in this Thesis

This thesis documents the first known investigation into HF MIMO communications, and provides several novel contributions.

A technique for estimating HF MIMO capacity from oblique ionogram images was developed and applied to images supplied by the DSTO. This exercise was important in gaining an initial estimate of HF MIMO capacity before proceeding further with the investigation.

A model for the HF MIMO channel matrix was developed. This model is important as it demonstrates the impact of antenna, mode correlation, and antenna spacing on channel matrix structure and rank, and hence capacity.

An MCR was developed. This receiver performs direct digital sampling, down conversion, and data logging on multiple channels simultaneously, and was used to record data used in HF MIMO capacity calculations. This receiver will be a valuable tool for conducting future HF MIMO research.

A technique for estimating HF MIMO capacity from recorded multi-channel data was developed and applied to data recorded with the MCR. The technique is an alternative to the approach involving direct recording of channel matrices, and has many advantages which have already been described. The technique yields a more accurate estimate of HF MIMO capacity compared with capacity estimation from ionogram images, since the MCR data offers a higher group delay resolution, allowing propagating modes with similar group delays to be distinguished, and because propagating mode correlation is taken into account in the calculations.

The overall aim of the investigation was to determine whether the HF band is suited to the application of spatial multiplexing techniques. The results obtained indicate that spatial multiplexing offers a significant increase in capacity compared with single channel communication techniques, and should therefore be seriously considered for future HF radio systems.

1.5 Publications

The following publications were generated throughout the course of the project:

1. N.L.Brine, C.C.Lim, A.D.Massie, and W.Marwood, ”Capacity estimation for the HF MIMO channel,” in *Sixth Symposium on Radiolocation and Direction Finding*, Southwest Research Institute, San Antonio, Texas, May 2006 (Chapters 5, 6, 7, 8, 9)

2. N.L.Brine, C.C.Lim, A.D.Massie, and W.Marwood, ”Estimation of multiple-input multiple-output capacity for the HF channel”, in *Workshop on Progress in Radar Research (PIRR)*, Adelaide, South Australia, November 2005 (Chapters 2, 5, 6, 7, 8, 9)

3. N.L.Brine, C.C.Lim, A.D.Massie, and W.Marwood, ”Measuring antenna correlation for the HF channel,” in *DCDIS 4th International Conference on Engineering Applications and Computational Algorithms*, Guelph, Ontario, July 2005 (Chapter 7).

4. N.L.Brine, C.C.Lim, A.D.Massie, and W.Marwood, ”HF multiple-input multiple-output capacity calculation using ionosonde data,” in *Seventh International Symposium on Digital Signal Processing and Communication Systems (DSPCS2003)*, Coolangatta, Queensland, Dec 2003 (Chapter 4).

5. N.L.Brine, C.C.Lim, A.D.Massie, and W.Marwood, ”A pre-emptive null-steering ionosonde,” in *Fourth Symposium on Radiolocation and Direction Finding*, Southwest Research Institute, San Antonio, Texas, May 2002 (Chapter 6).

Chapter 2

Background Material

Before investigating HF MIMO capacity, existing literature concerning capacity, spatial multiplexing, and the HF channel was studied. Background material on these topics is presented in this chapter. The chapter begins with an overview of capacity theory. The spatial multiplexing MIMO communication technique is then described, and the general MIMO capacity equation derived. The performance of spatial multiplexing in a rich multipath environment is demonstrated by making use of the general MIMO capacity equation and the Rayleigh channel model. The chapter concludes with a description of the properties of the HF channel.

2.1 Capacity

Capacity C of a communication channel is the transmission rate per unit bandwidth that represents the limit at which information can be transmitted without error, and is measured in bits per second per Hertz, or bps/Hz. If a transmission rate per unit bandwidth, or spectral efficiency, lower than that given by C is used, BER (bit error rate) can be made to approach zero through the use of coding. If on the other hand a spectral efficiency above C is used, BER cannot be made to approach zero. A practical communication system can only achieve, for a specified BER, a spectral efficiency that is some fraction of capacity.

For a memoryless wireless channel, which means that for each use of the channel an independent channel realization is drawn, with a transmit signal represented by the random variable X, and a receive signal represented by the random variable Y, instantaneous channel capacity

is defined as

$$C = \max_{p(X)} I(X;Y) \tag{2.1}$$

where $I(X;Y)$ is the mutual information between X and Y, and $p(X)$ is the range of possible distributions for X. Equation (2.1) states that capacity is given by the maximum mutual information between the transmitter and receiver over all possible transmit distributions.

Ergodic channel capacity is defined as

$$C = E_H\{\max_{p(X)} I(X;Y)\}$$

where $E_H\{.\}$ represents the expectation over all channel realizations.

Mutual information is a measure of the amount of information shared between two random variables, and can be expressed in terms of entropies as

$$I(X;Y) = h(X) - h(X|Y)$$

where $h(X)$ is the entropy of X, and $h(X|Y)$ is the conditional entropy betweeen X and Y. Entropy is a measure of the average amount of information carried by a variable, while conditional entropy is a measure of how much information carried by one variable remains, if the information carried by another variable has been completely learned.

To calculate ergodic capacity for the SISO case, an average power limitation P_T is imposed on the transmit signal x which reads

$$E\{|x|^2\} \leq P_T$$

where $E\{.\}$ is the expectation operator.

Ergodic capacity is given by

$$C = E_{h_{11}}\{\log_2(1 + \frac{P_T\,|h_{11}|^2}{\sigma_n^2})\} \tag{2.2}$$

where σ_n^2 is the AWGN (additive white Gaussian noise) power present at the receiver, and h_{11} is the random complex channel gain. This is the famous Shannon capacity equation [33], [34].

Another case to consider is that of the non-ergodic channel, where the channel realization is chosen randomly at the beginning of time and held fixed for all channel uses. In this case capacity is zero, since no matter how small the rate one attempts to communicate at, there is a non-zero probability that the channel realization will be incapable of supporting it regardless of code length. There is however a prescribed spectral efficiency or *outage capacity*, and a corresponding *outage probability* that gives the probability that the randomly selected channel will be able to support the prescribed level.

2.2 Spatial Multiplexing

Spatial multiplexing is a wireless communications technique which employs antenna arrays at both the transmit and receive ends to establish multiple parallel spatial data pipes within the same frequency band. The technique involves demultiplexing the stream of data symbols to be transmitted across the transmit antenna elements. Spatial signal processing is used at the receive end to recover the transmitted data symbol vectors, which are multiplexed back into a single stream. A simple diagram of a spatial multiplexing system is given in Figure 2.1.

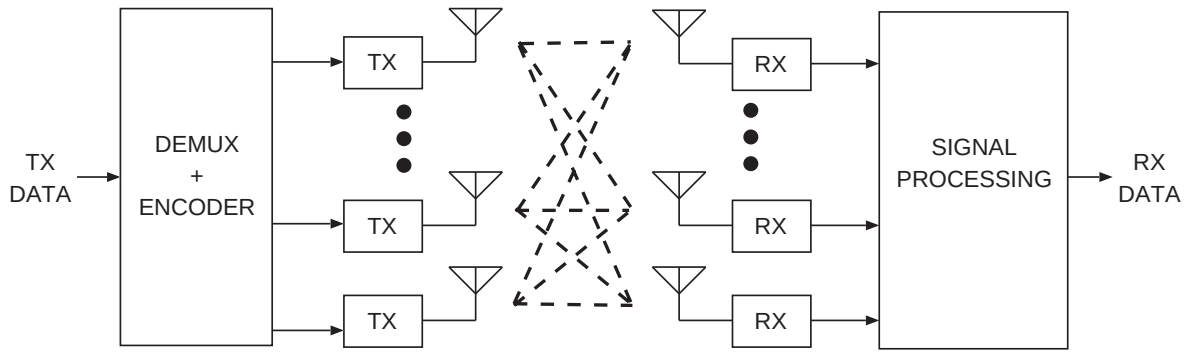

Figure 2.1. Diagram of a spatial multiplexing system

2.2.1 MIMO Capacity

The capacity offered by a MIMO wireless communication system employing spatial multiplexing is now considered. Much of the material presented in this section is based on the work of Telatar [1] and Holter [35].

If n_R represents the number of receive elements used, n_T represents the number of transmit elements used, and the transmitted signal bandwidth is narrow enough that the channel frequency characteristic can be considered flat across the band, the receive signal vector $\boldsymbol{y} \in \mathbb{C}^{n_R}$ is given by

$$\boldsymbol{y} = \boldsymbol{H}\,\boldsymbol{x} + \boldsymbol{\nu} \tag{2.3}$$

where $\boldsymbol{H} \in \mathbb{C}^{n_R \times n_T}$ is the channel matrix, the elements H_{ij} of which represent the complex transfer function between transmit element j and receive element i, $\boldsymbol{x} \in \mathbb{C}^{n_T}$ is the transmit signal vector, and $\boldsymbol{\nu} \in \mathbb{C}^{n_R}$ is the noise vector. Imposing an average transmit power limitation P_T, we have

$$\text{tr}(\boldsymbol{R}_{xx}) \leq P_T$$

where $tr(.)$ is the trace operator, $\boldsymbol{R}_{xx} \in \mathbb{C}^{n_T \times n_T} \equiv E\{\boldsymbol{x}\boldsymbol{x}^*\}$ is the transmit signal covariance matrix, and * is the conjugate transpose. If we assume $\boldsymbol{\nu}$ is an AWGN vector with iid (independent identically distributed) entries of power σ_n^2, the noise signal covariance matrix $\boldsymbol{R}_{\nu\nu} \in \mathbb{C}^{n_R \times n_R}$ is given by

$$\boldsymbol{R}_{\nu\nu} \equiv E\{\boldsymbol{\nu}\boldsymbol{\nu}^*\} = \sigma_n^2\,\boldsymbol{I}_{n_R} \tag{2.4}$$

where $\boldsymbol{I}_{n_R}$ is the $n_R \times n_R$ identity matrix.

To calculate ergodic MIMO capacity the following assumptions are made:

- $\boldsymbol{H}$ is random,
- the receiver has perfect channel knowledge, and
- each use of the channel corresponds to an independent realization of $\boldsymbol{H}$.

Under these assumptions, ergodic MIMO capacity is given by the expectation across all realizations of $\boldsymbol{H}$ of the maximum mutual information between $\boldsymbol{x}$ and $\boldsymbol{y}$ over all statistical

distributions of $\boldsymbol{x}$, $p(\boldsymbol{x})$, that satisfy the total power constraint

$$C = E_H\{\max_{p(\boldsymbol{x}):tr(\boldsymbol{R}_{xx})\leq P_T} I(\boldsymbol{x};\boldsymbol{y})\}.$$

Mutual information $I(\boldsymbol{x};\boldsymbol{y})$ is related to entropy by

$$I(\boldsymbol{x};\boldsymbol{y}) = h(\boldsymbol{y}) - h(\boldsymbol{y}|\boldsymbol{x})$$

where $h(.)$ is the differential entropy operator. Using (2.3) we can rewrite $I(\boldsymbol{x};\boldsymbol{y})$ as

$$\begin{aligned} I(\boldsymbol{x};\boldsymbol{y}) &= h(\boldsymbol{y}) - h(\boldsymbol{H}\,\boldsymbol{x} + \boldsymbol{\nu}|\boldsymbol{x}) \\ &= h(\boldsymbol{y}) - h(\boldsymbol{\nu}|\boldsymbol{x}) \\ &= h(\boldsymbol{y}) - h(\boldsymbol{\nu}). \end{aligned} \tag{2.5}$$

Equation (2.5) is maximised when the complex vector $\boldsymbol{y}$ is a circularly symmetric complex Gaussian to give

$$\max_{p(\boldsymbol{x}):tr(\boldsymbol{R}_{xx})\leq P_T} I(\boldsymbol{x};\boldsymbol{y}) = log_2[\det(\pi e R_{yy})] - log_2[\det(\pi e R_{\nu\nu})] \tag{2.6}$$

where $\boldsymbol{R}_{yy} \in \mathbb{C}^{n_R \times n_R} \equiv E\{\boldsymbol{y}\boldsymbol{y}^*\}$.

$\boldsymbol{R}_{yy}$ can be expressed as

$$\begin{aligned} \boldsymbol{R}_{yy} &= E\{(\boldsymbol{H}\boldsymbol{x} + \boldsymbol{\nu})(\boldsymbol{H}\boldsymbol{x} + \boldsymbol{\nu})^*\} \\ &= E\{\boldsymbol{H}\boldsymbol{x}\boldsymbol{x}^*\boldsymbol{H}^*\} + E\{\boldsymbol{\nu}\boldsymbol{\nu}^*\} \\ &= \boldsymbol{H}\boldsymbol{R}_{xx}\boldsymbol{H}^* + \boldsymbol{R}_{\nu\nu}. \end{aligned} \tag{2.7}$$

Substituting (2.4) and (2.7) into (2.6) we get

$$\begin{aligned}
\max_{p(\boldsymbol{x}):tr(\boldsymbol{R}_{xx})\leq P_T} I(\boldsymbol{x};\boldsymbol{y}) &= \log_2[\det(\pi e\boldsymbol{H}\boldsymbol{R}_{xx}\boldsymbol{H}^* + \boldsymbol{R}_{\nu\nu})] - \log_2[\det(\pi e\boldsymbol{R}_{\nu\nu})] \\
&= \log_2[\det(\boldsymbol{H}\boldsymbol{R}_{xx}\boldsymbol{H}^* + \boldsymbol{R}_{\nu\nu})] - \log_2[\det(\boldsymbol{R}_{\nu\nu})] \\
&= \log_2[\det((\boldsymbol{H}\boldsymbol{R}_{xx}\boldsymbol{H}^* + \boldsymbol{R}_{\nu\nu})(\boldsymbol{R}_{\nu\nu})^{-1})] \\
&= \log_2[\det(\boldsymbol{H}\boldsymbol{R}_{xx}\boldsymbol{H}^*(\boldsymbol{R}_{\nu\nu})^{-1} + \boldsymbol{I}_{n_R})] \\
&= \log_2[\det(\boldsymbol{H}\boldsymbol{R}_{xx}\boldsymbol{H}^*(1/\sigma_n^2)\boldsymbol{I}_{n_R} + \boldsymbol{I}_{n_R})] \\
&= \log_2[\det(\boldsymbol{H}\boldsymbol{R}_{xx}\boldsymbol{H}^*(1/\sigma_n^2) + \boldsymbol{I}_{n_R})].
\end{aligned}$$

The expression for MIMO capacity becomes [1]

$$C = E_H\{\max_{p(\boldsymbol{x}):tr(\boldsymbol{R}_{xx})\leq P_T} \log_2[\det(\frac{\boldsymbol{H}\boldsymbol{R}_{xx}\boldsymbol{H}^*}{\sigma_n^2} + \boldsymbol{I}_{n_R})]\}. \tag{2.8}$$

This equation is known as the general MIMO capacity equation. If the transmitter has no CSI (channel state information), then total power P_T is shared equally between each transmit antenna, to give $\boldsymbol{R}_{xx} = \frac{P_T}{n_T}\boldsymbol{I}_{n_T}$. The general MIMO capacity equation with no CSI is therefore given by

$$C = E_H\{\log_2[\det(\frac{P_T}{n_T\sigma_n^2}\boldsymbol{H}\boldsymbol{H}^* + \boldsymbol{I}_{n_R})]\}. \tag{2.9}$$

2.2.2 MIMO Capacity Expressed in Terms of Individual Channel Eigenmode Contributions

By performing a singular value decomposition of $\boldsymbol{H}$, (2.8) can be expressed as a summation of individual channel eigenmode contributions [6]. The singular value decomposition of $\boldsymbol{H}$ yields

$$\boldsymbol{H} = \boldsymbol{U}\boldsymbol{\Lambda}\boldsymbol{V}^* \tag{2.10}$$

where $\boldsymbol{U} \in \mathbb{C}^{n_R\times n_R}$ and $\boldsymbol{V} \in \mathbb{C}^{n_T\times n_T}$ are unitary, and $\boldsymbol{\Lambda} \in \mathbb{R}^{n_R\times n_T}$ has $r \leq \min(n_R, n_T)$ singular values $\lambda_1^{1/2}, \lambda_2^{1/2}, \cdots, \lambda_r^{1/2}$ on its main diagonal. If we set $\boldsymbol{R}_{xx}$ to

$$\boldsymbol{R}_{xx} = \boldsymbol{P}\boldsymbol{D}\boldsymbol{P}^* \tag{2.11}$$

where $\boldsymbol{D} \in \mathbb{R}^{n_T \times n_T}$ is a diagonal matrix containing the eigenvalues of $\boldsymbol{R}_{xx}$, and substitute (2.10) and (2.11) into (2.8), we get

$$C = E_H\{ \max_{p(\boldsymbol{x}):tr(\boldsymbol{R}_{xx}) \leq P_T} \log_2[\det(\frac{\boldsymbol{U\Lambda V^* PDP^* V\Lambda U^*}}{\sigma_n^2} + \boldsymbol{I}_{n_R})]\}.$$

By choosing $P = V$ we get

$$\begin{aligned}
C &= E_H\{ \max_{p(\boldsymbol{x}):tr(\boldsymbol{D}) \leq P_T} \log_2[\det(\frac{\boldsymbol{U\Lambda V^* VDV^* V\Lambda U^*}}{\sigma_n^2} + \boldsymbol{I}_{n_R})]\} \\
&= E_H\{ \max_{p(\boldsymbol{x}):tr(\boldsymbol{D}) \leq P_T} \log_2[\det(\frac{\boldsymbol{U\Lambda D\Lambda U^*}}{\sigma_n^2} + \boldsymbol{I}_{n_R})]\} \\
&= E_H\{ \max_{p(\boldsymbol{x}):tr(\boldsymbol{D}) \leq P_T} \log_2[\det(\frac{\boldsymbol{U\Lambda D\Lambda U^*}}{\sigma_n^2} + \boldsymbol{UU}^*)]\} \\
&= E_H\{ \max_{p(\boldsymbol{x}):tr(\boldsymbol{D}) \leq P_T} \log_2[\det(\boldsymbol{U}(\frac{\boldsymbol{\Lambda D\Lambda}}{\sigma_n^2} + \boldsymbol{I}_{n_R})\boldsymbol{U}^*\}]\} \\
&= E_H\{ \max_{p(\boldsymbol{x}):tr(\boldsymbol{D}) \leq P_T} \log_2[\det(\frac{\boldsymbol{\Lambda D\Lambda}}{\sigma_n^2} + \boldsymbol{I}_{n_R})\boldsymbol{UU}^*]\} \\
&= E_H\{ \max_{p(\boldsymbol{x}):tr(\boldsymbol{D}) \leq P_T} \log_2[\det(\frac{\boldsymbol{\Lambda D\Lambda}}{\sigma_n^2} + \boldsymbol{I}_{n_R})]\} \\
&= E_\lambda\{ \max_{\sum_{i=1}^r \gamma_i \leq P_T} \log_2[\prod_{i=1}^{r}(\frac{\lambda_i \gamma_i}{\sigma_n^2} + 1)]\} \\
&= E_\lambda\{ \max_{\sum_{i=1}^r \gamma_i \leq P_T} \sum_{i=1}^{r}(\log_2[\frac{\lambda_i \gamma_i}{\sigma_n^2} + 1])\}. \qquad (2.12)
\end{aligned}$$

The resulting equation expresses capacity as a summation of individual channel eigenmode contributions, where the value $r \leq \min(n_R, n_T)$ is the rank of the channel matrix $\boldsymbol{H}$ and represents the number of channel eigenmodes, λ_i are the eigenvalues of $\boldsymbol{HH}^*$ and represent the attenuation of each eigenmode, and γ_i are the eigenvalues of $\boldsymbol{R}_{xx}$ and represent the power allocated to each eigenmode.

2.2.3 Transmit Power Allocation

If full CSI is available at the transmitter, the optimal power allocation is given by waterfilling [36]

$$\gamma_i = (\mu - \frac{\sigma_n^2}{\lambda_i})^+ \qquad (2.13)$$

where $(x)^+ = \max(0, x)$. The water level μ is found by applying the total transmit power constraint

$$\sum_{i=1}^{r} \gamma_i = P_T. \tag{2.14}$$

Substituting (2.13) into (2.12), the capacity equation with full CSI at the transmitter becomes

$$C_{fullCSI} = \sum_{i=1}^{k} \log_2(\frac{\mu\lambda_i}{\sigma_n^2}) \tag{2.15}$$

where k is the number of nonzero power allocations γ_i.

If no CSI is available at the transmitter, then total transmitted power is divided equally between each eigenmode

$$\gamma_i = \frac{P_T}{n_T} \tag{2.16}$$

where it is assumed $r = n_T$. Substituting (2.16) into (2.12), the capacity with no CSI at the transmitter becomes

$$C_{noCSI} = \sum_{i=1}^{n_T} \log_2(1 + \frac{P_T}{\sigma_n^2 n_T}\lambda_i). \tag{2.17}$$

If all eigenmodes are of the same quality, $\lambda_1 = \lambda_2 = \ldots = \lambda_n$, capacity with and without CSI is the same. Furthermore, as P_T/σ_n^2 increases, capacity with no CSI at the transmitter approaches capacity with full CSI at the transmitter, irrespective of the relative quality of each eigenmode.

2.2.4 Simulating the MIMO Channel

The Rayleigh channel model is often used to model channels rich in multipath scattering [1], [4]. By using this model to generate realizations of the random $\boldsymbol{H}$, we can calculate the approximate ergodic capacity offered by rich scattering channels. The Rayleigh channel model yields channel matrix entries H_{ij} given by

$$\begin{aligned} H_{ij} &= \mathcal{N}(0, \frac{1}{\sqrt{2}}) + j\ [\mathcal{N}(0, \frac{1}{\sqrt{2}})] \\ &= \mathcal{CN}(0, 1) \end{aligned}$$

where $\mathcal{N}(\mu, \sigma^2)$ is the Gaussian distribution with mean μ and variance σ^2, and $\mathcal{CN}(\mu, \sigma^2)$ is the complex Gaussian distribution with mean μ and variance σ^2. The variance of the distribution is set to 1 such that $E\{|H_{ij}|^2\} = 1$, and channel energy is given by the Frobenius norm of $\boldsymbol{H}$, $||\boldsymbol{H}||_F^2 = tr(\boldsymbol{H}\boldsymbol{H}^*) = n_R n_T$.

Ergodic capacity was computed for the Rayleigh channel model using (2.9), setting $n = n_T = n_R$, SNR (signal-to-noise ratio) $\rho = (P_T/\sigma_n^2) = [-5 : 5 : 25]$ dB, where the notation $[i : n : j]$ represents $[i, i+n, i+2n, \ldots, j]$, and using 1000 $\boldsymbol{H}$ realizations, with the plot shown in Figure 2.2. From the plot we see capacity increases linearly with increasing n, while the slope of the capacity plot steepens with increasing ρ. A Rayleigh distributed channel matrix of size $n \times n$ has n linearly independent rows or columns, and is thus of rank n. The corresponding term $\boldsymbol{H}\boldsymbol{H}^*$ has n eigenmodes. The plot in Figure 2.2 is an indication of a linear relationship between capacity and the rank of the channel matrix. Maximum channel matrix rank is related to the amount of multipath in the channel, and represents the number of parallel spatial data pipes that can be supported. A rich multipath channel offering a large maximum channel matrix rank is well suited to spatial multiplexing, however it should be noted that a rich multipath channel does not necessarily guarantee a large maximum channel matrix rank [37].

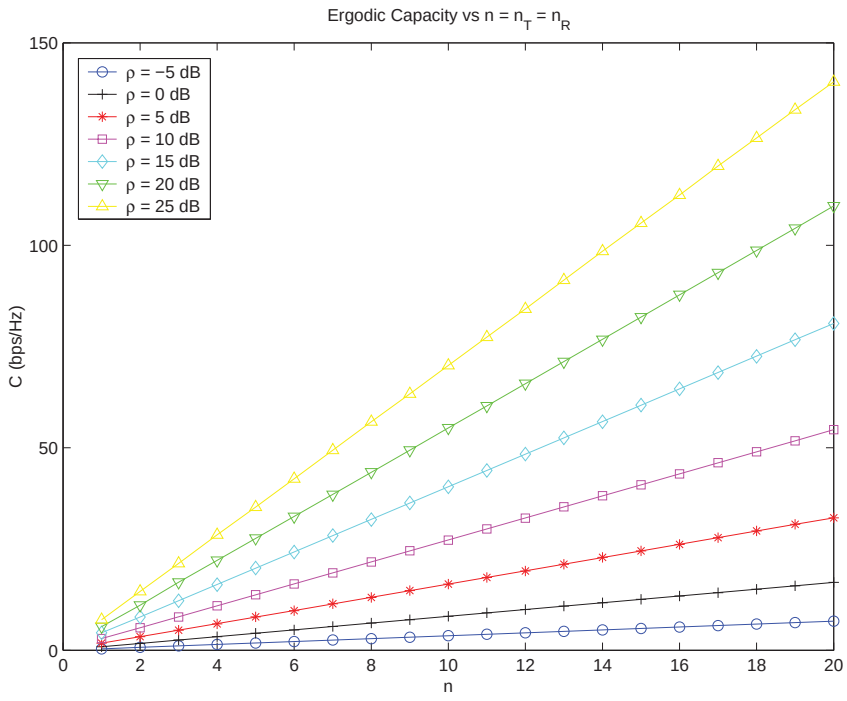

Figure 2.2. Ergodic capacity versus $n = n_T = n_R$

For the non-ergodic case we use the CCDF (complementary cumulative distribution function) of capacity [4], which gives the probability that a random channel can support a prescribed spectral efficiency. By plotting the CCDF of capacity, a detailed picture of outage capacity can be obtained. The CCDF of capacity was calculated for the Rayleigh channel model using (2.9), setting $n = n_T = n_R = [4 : 2 : 20]$, $\rho = (P_T/\sigma_n^2) = [0 : 5 : 25]$ dB, CCDF x-axis step size to 0.01 bps/Hz, CCDF y-axis lower limit to 0.9, and using 1000 $\boldsymbol{H}$ realizations. Plots of the CCDF of capacity are shown in Figure 2.3

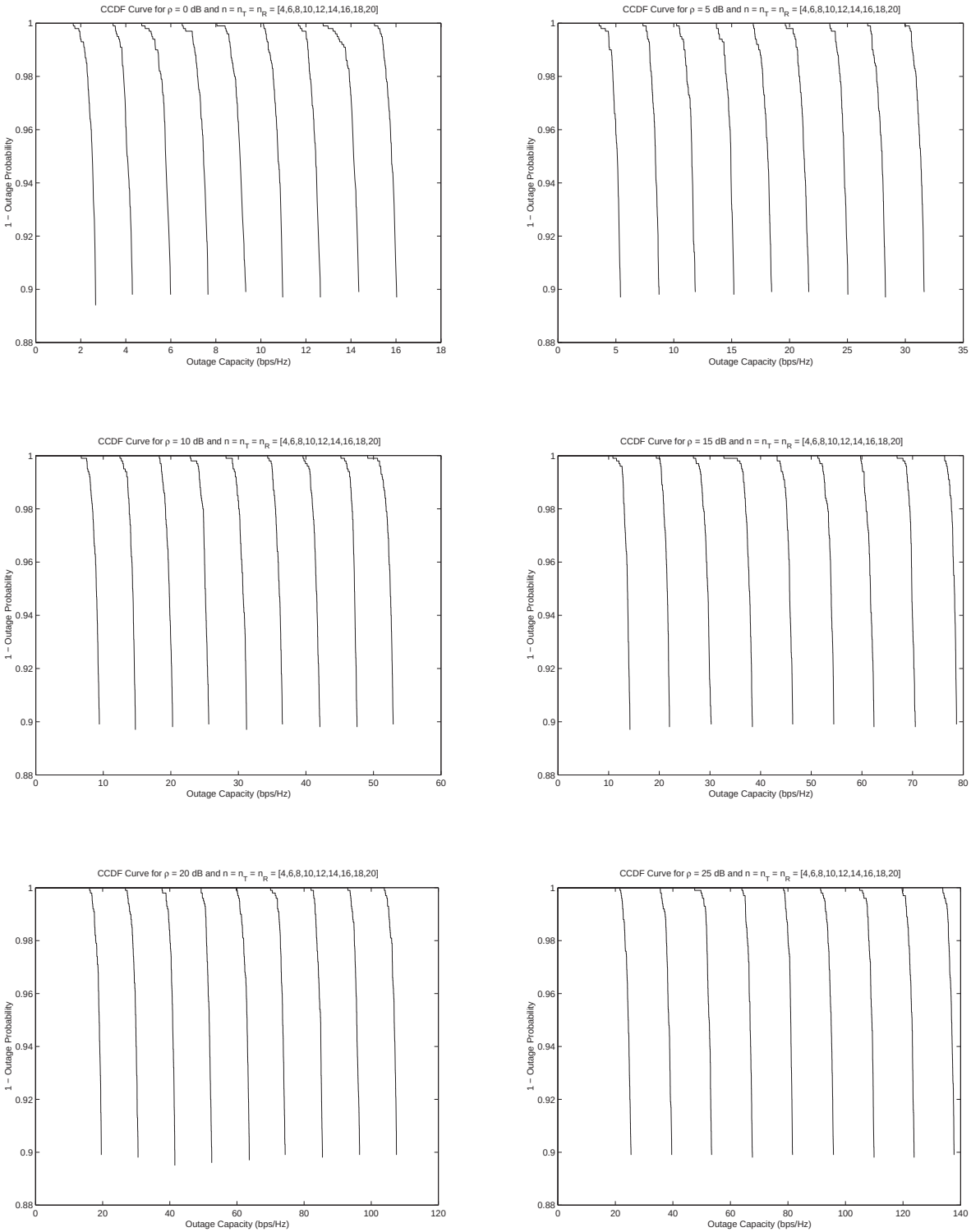

Figure 2.3. Plots of CCDF of capacity

2.3 The HF Band

In the last subsection MIMO capacity was shown to increase linearly with maximum channel matrix rank. Rich multipath channels tend to offer a large maximum channel matrix rank and so are generally well suited to the application of spatial multiplexing techniques. The HF band is subject to significant multipath and may therefore be a suitable candidate for spatial multiplexing.

The HF band is typically defined as the band of frequencies ranging between 3 and 30 MHz [38], which propagate via the ionosphere [39], [40], [41]. The ionosphere is a section of the atmosphere that is ionized by solar radiation. The free electrons resulting from the ionization process causes the refraction of incident HF radio waves back to earth. The degree of ionization affects the maximum frequency of waves which are refracted, termed the MUF (maximum usable frequency), and the level of ionization is dependent on the amount of solar radiation received from the sun. Ionization and the MUF thus vary according to time of day, month of year, and sunspot number.

The main layers of the ionosphere are the D, E, and F layers.

2.3.1 D Layer

The D layer is the lowest layer of the ionosphere, located 50-90 km above the surface of the earth. Because the level of ionization is low, HF radio waves are not refracted by this layer. Instead, HF radio waves with frequencies of the order of 10 MHz and below are absorbed by this layer, with absorption levels low at night, and greatest at around noon. The amount of absorption caused by the D layer reduces progressively for waves of increasing frequency.

2.3.2 E Layer

The E layer is the middle layer of the ionosphere, located 90-120 km above the surface of the earth. This layer refracts HF radio waves with frequencies of the order of 10 MHz and below, and partially absorbs waves of higher frequencies. The E layer comes closer to the earth during the day and moves away from the earth during the night, so transmission range is increased during the night.

2.3.3 F Layer

The F layer is the outermost layer of the ionosphere, located 120-400 km above the surface of the earth. During the day the F layer splits into two layers F_1 and F_2, while at night the two layers merge to form a single layer. The F layers are responsible for most long range HF radio propagation.

2.3.4 Multipath in the HF channel

The HF band is subject to significant multipath caused by multiple refractions and reflections, or *hops*, between the ionospheric layers and the earth's surface. These multiple paths are referred to as the propagating modes. The diagram in Figure 2.4 shows how a simple 1-hop and 2-hop path can give rise to multipath.

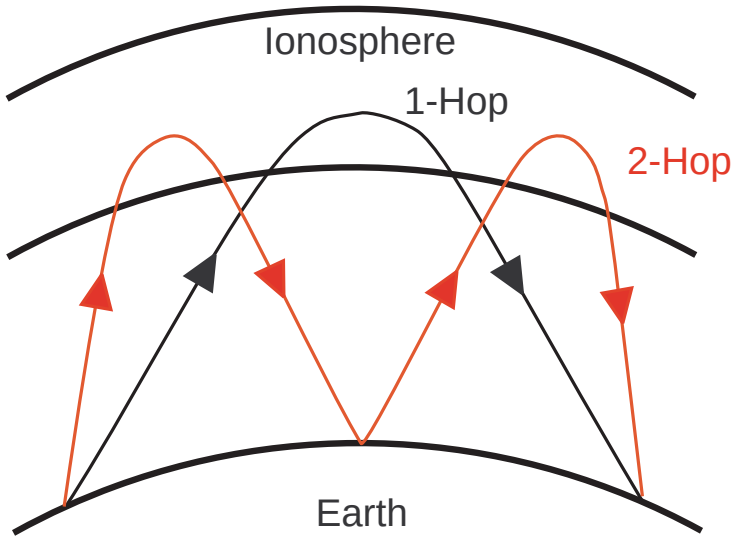

Figure 2.4. Multipath in the HF band due to multiple hops

2.3.5 Ionospheric sounding

Ionospheric sounding is used to measure the state of the ionosphere. The transmit and receive systems used for ionospheric sounding are called *ionosondes*, while the recorded data plots are called *ionograms*. Ionospheric sounding may be either vertical or oblique. Vertical sounding employs a co-located transmitter and receiver, while oblique sounding uses a separate transmitter and receiver which are synchronized via GPS. Sounding techniques include both pulsed and FMCW. FMCW techniques offer both lower power and better sensitivity compared with the pulsed alternative.

Ionogram plots show the different modes of propagation present across the entire range of HF frequencies and the corresponding group delays. A depiction of an oblique ionogram with 1-hop, 2-hop and 3-hop propagating modes is shown in Figure 2.5, while a plot of a real oblique ionogram recorded using the MCR is shown in Figure 2.6.

The Australian Space Weather Agency [42] is an example of a group that provides up to date ionograms which can be consulted by radio operators when selecting a suitable frequency of operation.

For more information on ionospheric sounding consult [43].

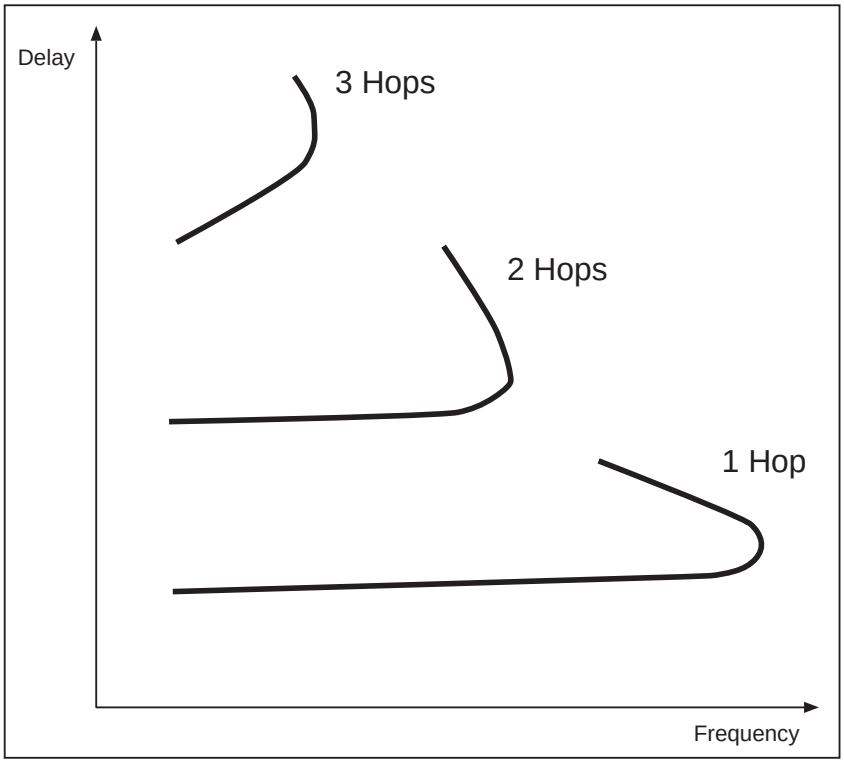

Figure 2.5. A depiction of an ionogram for a channel with 1-hop, 2-hop and 3-hop propagating modes

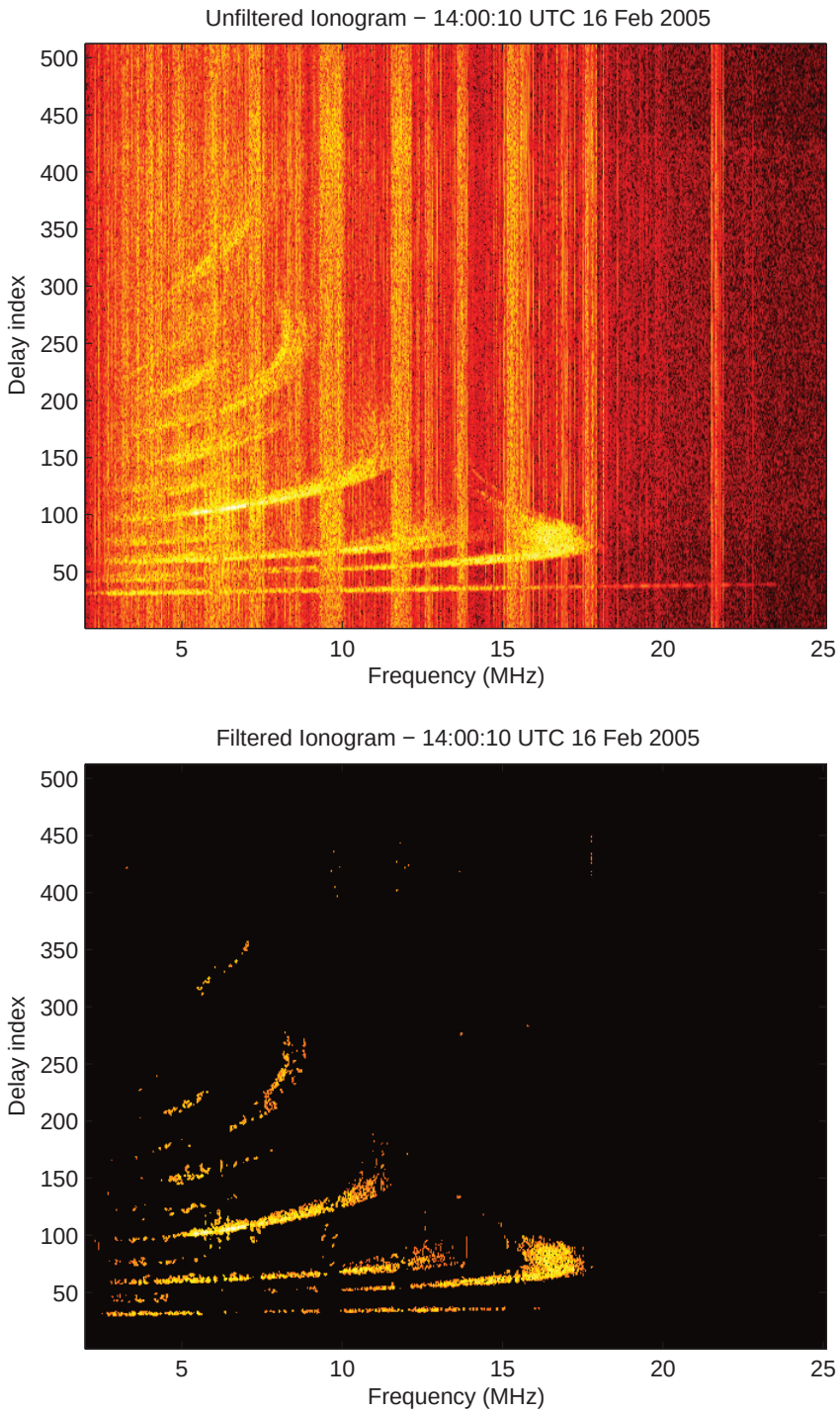

Figure 2.6. An ionogram recorded using the MCR

Chapter 3

Literature Survey

A survey of research literature concerning wireless MIMO communication systems was performed in order to determine the current state of research in this field, and to gain knowledge of existing approaches used to measure MIMO capacity. The survey included a search for material on HF MIMO communications. The details of the literature survey are presented in this chapter.

To begin, a timeline of MIMO developments is provided in Figure 3.1. The first discovery of the enormous potential of spatial multiplexing was made in late 1995 by Telatar and published in an internal Bell Laboratories technical report. Shortly following this, in 1996, Foschini published an article in the Bell Laboratories Technical Journal describing a spatial multiplexing technique called BLAST (Bell Laboratories layered space-time). In 1998 a team of Bell Laboratories researchers had successfully implemented a modified version of the BLAST architecture called V-BLAST (vertical BLAST). By the year 2000, MIMO had become a hot research topic driven by the enormous commercial potential for high data rate wireless LAN and personal communication devices. In late 2004 the first wireless LAN equipment featuring spatial multiplexing was released to the public using a chipset produced by Airgo Networks [44].

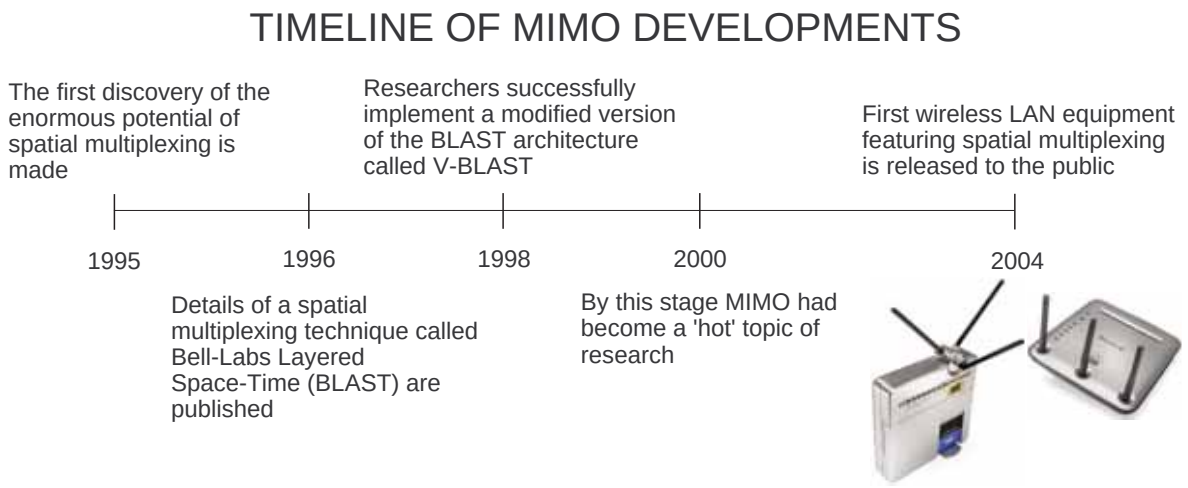

Figure 3.1. A timeline of MIMO developments

3.1 MIMO Capacity Theory

MIMO communication was first investigated in [1], [2] and [4]. It was Telatar in [1] who derived the general MIMO capacity equation (2.8) for a memoryless channel, where each channel usage corresponds to an independent channel realization, and capacity is given by the maximum mutual information. He found that mutual information is maximised by a transmit signal vector which is circularly symmetric complex Gaussian with zero mean. Telatar analysed the general MIMO capacity equation by assuming Rayleigh distributed channel matrix entries, expressing capacity in terms of the eigenvalues of the channel covariance matrix, and subsequently deriving an integral expression for capacity. This analytical approach is an alternative to the monte-carlo approach taken in Section 2.2.4. The results of this analysis show that MIMO capacity increases linearly with the number of transmit and receive antennas used. Telatar also considered the non-ergodic channel case where the channel realization is chosen randomly at the beginning of time and held fixed for all channel uses. In this case capacity is zero since no matter how small the rate one attempts to communicate at, there is a non-zero probability that the channel realization will be incapable of supporting it regardless of code length. In this situation there is however a prescribed spectral efficiency, or *outage capacity*, and a corresponding *outage probability* that gives the probability that the randomly selected channel will be able to support the prescribed level. For the non-ergodic channel case, Telatar determined the optimal

structure for the transmit signal vector and showed that using fewer transmit antennas is preferable for very high outage capacities and corresponding high outage probabilities. Telatar did not offer a technique or architecture for realizing the large MIMO capacities predicted by the general MIMO capacity equation.

In [2] Foschini analysed the general MIMO capacity equation for n transmit and receive antennas using the Rayleigh channel model and obtained plots of capacity versus n by means of the monte-carlo approach taken in Section 2.2.4 to show that MIMO capacity increases linearly with the number of transmit and receive antennas. A lower bound for MIMO capacity was specified in terms of n independent chi-squared variates. Comparing this with capacity for a (1,n) receive diversity system suggested that one may combine $n \times (1, n)$ receive diversity systems to form an (n, n) MIMO system. Subsequently, Foschini was able to devise a MIMO codec (coder decoder) architecture for achieving a significant fraction of the general MIMO capacity equation, which is now known as the BLAST architecture. Foschini showed that the BLAST architecture achieves a capacity equal to the capacity lower bound expressed in terms of n independent chi-squared variates. He also analysed the capacity per dimension measure which affects signal constellation complexity, and showed that capacity per dimension and hence signal constellation complexity remains reasonable, even for large overall capacities.

The BLAST transmission technique involves demultiplexing the single data stream into n data streams of equal rate. The association between data streams and transmit antennas is cycled periodically, such that each stream gets equal use of all channel paths and neither of the streams is stuck with the worst of the n antennas. In addition, each data stream has the same capacity, leading to uniform encoding and decoding for each stream. Because the same signal constellation is used for each stream, maximum constellation complexity is minimized.

Processing at the receive end relies upon knowledge of the channel matrix, which is estimated using a training sequence. To detect a symbol transmitted by one particular antenna, interference caused by the other transmit antennas needs to be removed. In detecting the symbol from the first antenna, the $n-1$ interfering signals from the other transmit antennas are removed by projecting the receive signal vector into the maximal subspace orthogonal to the subspace spanned by signals from all other transmit antennas. Once the symbol from the first antenna has been estimated, it can be cancelled from the signal vector. Detection of the symbol from the next transmit antenna involves processing of the signal vector with the symbol from the first transmit antenna cancelled, so nulling of only $n - 2$ interfering signals is required. Detection

of the symbol from the final antenna requires no nulling, since symbols from all other transmit antennas have been estimated and cancelled from the receive signal vector.

In [4], which is a companion article to [2], the capacity lower bound expressed in terms of n independent chi-squared variates was derived. Plots of the CCDF of capacity were also provided, which give a detailed picture of outage capacity for the non-ergodic channel, following the monte-carlo approach taken in Section 2.2.4.

3.2 First Implementation of a Spatial Multiplexing System

Details of the first ever implementation of a spatial multiplexing system were provided by a team of Bell Labs researchers in [5]. The implemented architecture is a simplified version of BLAST called V-BLAST, in which the association between data streams and transmit antennas is fixed. The processing at the receive end to detect the symbols from each transmit antenna is similar to that described in [2], where a combination of cancellation of already detected symbols, and nulling of yet to be detected symbols, is applied to the receive signal vector. The performance of the technique is dependent on the order that transmit symbols are detected. It is shown that optimal performance is achieved by selecting the symbol offering the highest post-detection SNR at each symbol detection stage. The implemented system comprises 8 transmit antennas and 12 receive antennas separated by $\lambda/2$ (where λ is the wavelength), features a carrier frequency of 1.9 GHz, a burst length of 100 symbol durations (20 of which are used to estimate the channel matrix at the receive end), a transmit signal power adjusted to give an average receive SNR of 24 dB, and employs an uncoded 16-QAM (quadrature amplitude modulation) constellation on each individual transmit stream, to give a resulting data rate of 621 kbps in a 30 kHz bandwidth, corresponding to a spectral efficiency of 20.7 bps/Hz. BER for the system is around 10^{-5} which can be further improved through the use of error correcting codes.

3.3 MIMO Capacity Investigations Using Ray Tracing Techniques

In Section 2.2.4 we saw that the general MIMO capacity equation can be simulated by using the Rayleigh channel model to generate the entries of the channel matrix. The Rayleigh channel

model is an idealistic multipath model which yields a full rank channel matrix, such that channel matrix rank and hence capacity is dependent on the number of transmit and receive antennas used. In reality the number of channel eigenmodes, or maximum channel matrix rank, is limited by properties of the channel such as multipath, and correlation between antennas.

Following the work of Telatar and Foschini, researchers were interested in determining the maximum capacity offered by MIMO systems. The main techniques devised to improve on estimates obtained using the Rayleigh channel model were ray tracing simulations and channel matrix measurements.

In [7] a ray tracing tool called WiSE (Wireless Systems Engineering)[2] was used to generate channel matrices for a MIMO system operating at a carrier frequency of 1.9 GHz. Two different scenarios were considered.

The first scenario featured transmit and receive antenna arrays of 16 elements arranged as 4×4 square grids, situated inside an office building. The transmit array was placed at a fixed position on the ceiling of the building corridor, while the receive array was placed at numerous test locations at desktop height in three rooms, each of increasing distance from the transmitter. CCDF plots of capacity were generated for each of the three rooms with antenna element spacing set to $0.5\ \lambda$, peak transmit power set to 20 dBm and 23 dBm, and noise power set to 100.8 dBm. With signal and noise powers calibrated in a 10 MHz bandwidth, and for a peak transmit power of 20 dBm, the 5% outage capacity was found to be 167.7 bps/Hz for the room closest to the transmitter, 66.9 bps/Hz for the second room, and 24.3 bps/Hz for the furthest room. With the receiver placed in the second room, antenna element separation was increased from $0.5\ \lambda$ to 1, 2, and $3\ \lambda$. Channel rank was found to increase by two when antenna element separation was increased from $0.5\ \lambda$ to $3\ \lambda$.

The second scenario featured transmit and receive antenna arrays of just 4 elements in size situated in an outdoor environment based on Rosslyn City, Virginia. The transmit array was placed in a fixed position on the top of a building, while the receive array was placed at numerous test locations on top of other buildings. Transmit antenna element separation was set to $3\ \lambda$, while receive antenna element separation was set to $1\ \lambda$. The authors experienced problems with the amount of computation required by WiSE to simulate the outdoor environment, and used a first-order approximation to the outdoor propagation model. CCDF plots of capacity

[2]The WiSE tool allows the layout of both indoor and outdoor environments to specified, and generates the corresponding propagation models. The reflection and refraction coefficients and scattering effect for different building materials are derived from a multilayer dielectric model [45].

were generated with peak transmit power varied between 17 dBm, 20 dBm, and 23 dBm. For a peak transmit power of 17 dBm, the $(n_r, n_t) = (4, 4)$ system achieved a 5% outage capacity of 15.5 bps/Hz, compared to 5.6 bps/Hz for a single antenna system. A peak transmit power of 20 dBm gave a capacity of 18.3 bps/Hz, while a peak transmit power of 23 dBm gave a capacity of 21.3 bps/Hz.

In [46] an outdoor city environment was modelled using wedges to represent building edges and rectangular planes to represent building walls. Ray tracing was performed in order to demonstrate that for certain transmit and receive array positions, channel matrix rank can be collapsed to 1, in which case spatial multiplexing is no longer effective. Such a channel is referred to as a *keyhole* [37].

In [8] the work of [7] was extended to analyze the impact of fading correlation in an indoor environment, and once again WiSE was used. For each MIMO system setup considered, the transmitter was located in a corridor and the receiver was located in an adjacent room. The first setup considered was a $(n_r, n_t) = (2, 2)$ system. Transmit and receive correlation was measured as antenna element separation was varied. The plots show that the magnitude of antenna correlation resembles slow decaying zero-ordered Bessel functions, and that transmit correlation was much higher than receive correlation. This was because of the different fading statistics of the corridor compared with the room.

The second setup considered featured antenna arrays arranged as grids of $n_r = n_t = 1$, 4, 9, 16, 25 and 36 elements, with element spacing set to 0.5 λ. For this setup capacity with and without the use of waterfilling (as described in Section 2.2.3) was measured. For a carrier frequency of 5.2 GHz and a receive SNR of 18 dB in a bandwidth of 10 MHz, the fractional gain of using waterfilling over an equal-power allocation was found to vary from 0 for $n_r = n_t = 1$, up to 11.3% for $n_r = n_t = 36$. Additional measurements were performed which showed that the fractional gain of using waterfilling over an equal-power allocation increases as receive SNR is reduced.

The third setup involved a comparison between an approximately independent fading situation where transmit and receive arrays have elements placed at iid random locations and a correlated fading situation where transmit and receive arrays are linear with element spacing set to 0.5 λ and 5 λ. The effect of correlation was found to be substantial, even for the element spacing of 5 λ. With receive SNR set to 22 dB, and $n_r = n_t = 16$, a 5 λ spacing

gave approximately 90% of the capacity achieved by the system featuring elements placed at iid random locations.

In [47] the effects of complex wall structures on fading characteristics and MIMO capacity was investigated using an FDTD (finite difference time domain) method. Complex wall structures were found to offer higher MIMO capacity and improved coverage when compared with slab and effective slab walls. Such a finding stresses the importance of detailed modeling of wall structures for accurate characterization of the indoor fading channel.

Further examples of research literature concerned with MIMO communications and ray tracing include [48], [49], [50], [51] and [52].

3.4 MIMO Capacity Investigations Involving Channel Matrix Measurements

Ray tracing techniques provide a simple means of designing MIMO systems and investigating MIMO capacity. The advantage of such techniques is that a MIMO system does not need to be built which is a costly and tedious task. The disadvantage however is that the accuracy of the results obtained are dependent on propagation modelling. In [47] it was shown that modelling complex walls as effective slabs will underestimate capacity, while in [53] the use of the plane-wave assumption was shown to underestimate MIMO channel matrix rank and hence capacity when an LOS (line-of-sight) path is present. In addition, when performing ray tracing calculations for outdoor environments, the amount of computation required can be prohibitive [7].

Despite the cost and effort required to build a MIMO system for channel matrix estimates, the benefit is obvious. Because a true channel matrix measurement is made, the corresponding capacity measurement is exact, subject to the transmit signal vector and receive noise vector being circularly symmetric Gaussian. The disadvantage however is that channel matrix rank and capacity are limited by the number of transmit and receive elements used, and if the number of underlying channel eigenmodes is greater than the dimensionality of the designed MIMO system, the maximum capacity potential of the channel cannot be determined. If on the other hand the number of transmit and receive elements used is greater than the number of underlying channel eigenmodes, the point on the graph of capacity versus $n = n_r = n_t$ where capacity

changes from a linear growth to a log growth, will be observable. This corresponds to the point where the full spatial multiplexing capacity gain has been realized, and adding extra antennas only provides array gain.

In [9] the first details of a practical MIMO capacity investigation using channel matrix measurements were provided. The system designed to make the channel matrix measurements featured transmit and receive antenna arrays with 16 elements, a carrier frequency of 2.11 GHz, and a transmit power of 20 dBm per element. The transmit elements were arranged as a 3 m long horizontal linear array of 8 pairs of elements, with each pair comprising a vertically polarized and a horizontally polarized element. Exploiting polarization diversity in this way is beneficial because it results in a more compact antenna array [54]. The receive elements were arranged as a grid in the vertical plane with alternating element polarizations and an inter-element separation of $\lambda/2$. The transmit array was placed at an elevated position 100 m above street level in order to represent a typical base station position, while the receive array was mounted on a van at a height of 1.5 m which is indicative of the height a personal communication device is likely to be used. The positioning of the transmit and receive antennas is important because an elevated base station antenna array will experience reduced scattering leading to lower channel matrix rank and hence capacity [55]. Each transmit element was used to transmit a unique continuous wave pulse which was identified at the receive end using FFT processing. Synchronization between the transmit and receive arrays was achieved using GPS. The van was driven at speed of 20 mph, as channel matrix measurements were taken at a rate of 650 times per second. The measured channel matrices were inserted into the general MIMO capacity equation with no CSI (2.9) to give capacity. At a 50% outage level, an $(n_r, n_t) = (2, 2)$ system was found to achieve 99% of the capacity given by the Rayleigh channel model, compared with 95% for an $(n_r, n_t) = (4, 4)$ system, and 77% for an $(n_r, n_t) = (16, 16)$ system. Capacity of the $(n_r, n_t) = (16, 16)$ was shown to deteriorate substantially as the outage level was decreased.

Another example of a practical MIMO capacity investigation is documented in [10]. The system designed to take the channel matrix measurements in this case featured 8 transmit antenna elements and 4 receive antenna elements and operated at a carrier frequency of 2.14 GHz. Two different receive antenna array setups were used, a handset receive array and a laptop receive array. The handset receive array featured four patch antennas located at the corners, with a horizontal spacing of 0.25 λ and a vertical element spacing of 0.5 λ. The laptop receive array featured four elements in a linear arrangement with a spacing of 0.5 λ. The arrangement of the transmit antenna array elements was not specified. The transmit array was placed at various

positions inside a building, while the receive arrays were placed at various indoor and outdoor positions. With the receive arrays placed inside, total transmit power was set to -16 dBm, and this was boosted to +14 dBm when the receive arrays were placed outside. The transmitted signals employed a code phase offsetting technique with a PRBS (pseudo-random binary sequence) sequence of length 511 bits and a chip rate of 7.665 MHz. At the receive end, data from each antenna was sampled at a rate of 15.36 MHz and recorded to a hard drive. The data was post-processed on a computer in order to obtain the channel matrices. Receive antenna correlation was measured between different pairs of antennas. The rectangular handset array featured spacings of 0.25 λ, 0.5 λ and 0.75 λ, and measured correlation was found to be independent of element separation for these values. Practical factors such as mutual coupling and differences in antenna radiation patterns were suggested as reasons for this. Capacity with and without CSI available at the transmitter was calculated from the obtained channel matrices, and comparisons were made with capacity for the Rayleigh distributed channel matrix. For a 20 dB SNR, obtained channel matrices were found on average to give 80% of the capacity of a Rayleigh distributed channel matrix. The use of CSI was found to be important at low SNRs. For a 20 dB SNR, capacity with CSI available at the transmitter was found to be up to 20% higher than capacity with no CSI available at the transmitter.

Further examples of research literature concerned with MIMO channel measurements include [56], [57], [58], [59] and [60].

3.5 MIMO Capacity Models

The development of MIMO capacity models is important since it can provide a MIMO communication systems designer with a simple means of estimating capacity. One such model is proposed for the outdoor environment by Gesbert et al in [27]. Parameters for the proposed model include the wavelength of the transmitted signals, scattering cloud radii at transmit and receive ends, distance between transmit and receive arrays, antenna beamwidths, and antenna spacing. The proposed model encompasses three important classes of MIMO channels, uncorrelated high rank, where the elements of the channel matrix are Rayleigh distributed, uncorrelated low rank, where spatial diversity is present but there is no multiplexing gain, and correlated low rank, where there is no diversity or multiplexing gain, only receive array gain. Verification

of the proposed model is performed through comparison with a ray tracing model. Capacity distributions given by the two models were found to be within 1 bps/Hz for all cases examined.

Further examples of research literature concerning MIMO capacity models include [61], [62], [63], [64], [65], [66], [67] and [68].

3.6 HF MIMO Systems

A search for literature on HF MIMO communications was conducted, and yielded a paper in which an HF communication scheme featuring two transmit and receive antennas is proposed [69]. The scheme involves transmitting the same symbols on the two transmit antennas to give improved resistance to fading, and diversity gain. The paper also suggests the possibility of applying both spatial multiplexing and OFDM (orthogonal frequency division multiplexing) techniques in the HF band, however no actual investigation into these suggestions is performed. The work presented in this thesis is the first known investigation into HF spatial multiplexing communications to be performed. Just prior to the submission of this thesis, additional research into HF MIMO communications started to appear [21], [22], [23], [24], [25], [26].

3.7 MIMO Techniques Requiring No Knowledge of the Channel at the Receiver

Finally we mention a MIMO space-time modulation scheme called unitary space-time modulation which does not require an estimate of the channel matrix at the receive end [70], [71]. Such a scheme is appropriate for situations where the time required to estimate the channel matrix is large compared with the fading interval, which may be the case for the HF channel. In Chapter 7 a technique for measuring time correlation of the HF channel is described. Such a measure gives an indication of the rate at which the HF channel matrix varies with time, and can therefore be used to determine whether a technique such as unitary space-time modulation is appropriate. Plots of path length variation versus sample number, which are presented in Chapter 8, suggest that the HF channel matrix is indeed fast time varying. Further investigation into time variation of the HF channel matrix is required, as discussed in Chapter 9.

Chapter 4

Calculation of HF MIMO Capacity Using Ionosonde Data

The first step for the HF MIMO capacity investigation that is the subject of this thesis was to perform capacity calculations on an existing set of HF radio data. This step allowed an insight to be gained into the level of HF MIMO capacity available before proceeding with the development of the MCR to be used for HF radio data collection. The existing set of HF radio data used was collected using the LLISP network of oblique FMCW ionosondes, which comprises a single receiver located in Darwin, and several transmitters located in Northern Australia and South-East Asia, and was established by DSTO for HF radio research purposes.

4.1 Details of the LLISP Network

The LLISP ionosonde receiver is located in Darwin, while the LLISP ionosonde transmitters are located in Saipan, Vanimo, Manila, Tennant Creek, Cocos Keeling, Townsville and Eleven Mile[3]. These locations are marked with dots on the map shown in Figure 4.1. Specifications for the LLISP network are provided in Table 4.1. More information about the LLISP network can be found in [72], [73] and [74].

[3]The Eleven Mile transmitter is located eleven miles from the Darwin receiver, and is used to measure the vertical path.

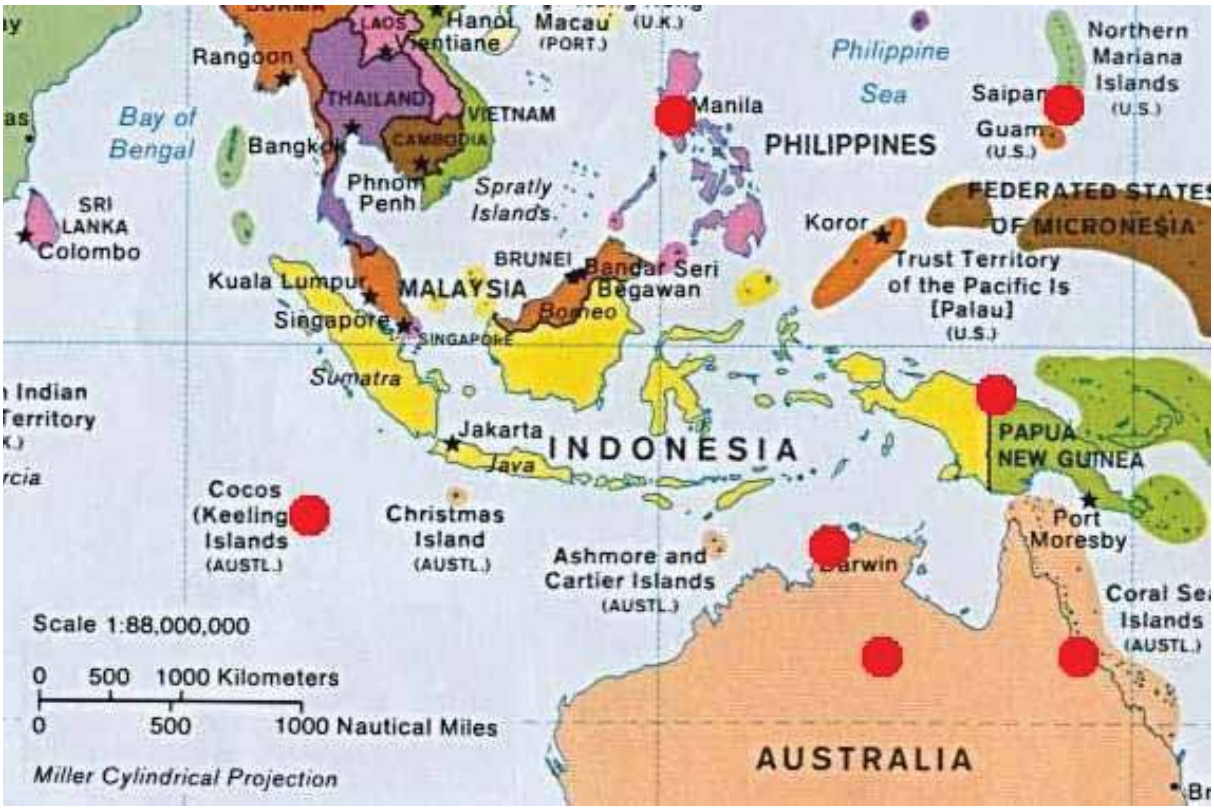

Figure 4.1. A map showing the locations of the LLISP ionosonde transmitter and receivers

4.2 HF MIMO Capacity Calculation

The approach taken to calculate HF MIMO capacity uses equations which were derived in Chapter 2.

The general MIMO capacity equation (2.8) was found to be

$$C = E_H\{\max_{p(\boldsymbol{x}):tr(\boldsymbol{R}_{xx})\leq P_T} \log_2[\det(\frac{\boldsymbol{H}\boldsymbol{R}_{xx}\boldsymbol{H}^*}{\sigma_n^2} + \boldsymbol{I}_{n_R})]\}.$$

MIMO capacity in terms of individual channel eigenmode contributions (2.12) was found to be

$$C = E_\lambda\{\max_{\sum_{i=1}^r \gamma_i \leq P_T} \sum_{i=1}^{r}(\log_2[\frac{\lambda_i\gamma_i}{\sigma_n^2} + 1])\}$$

where the value $r \leq \min(n_R, n_T)$ is the rank of the channel matrix $\boldsymbol{H}$ and represents the number of channel eigenmodes, λ_i are the eigenvalues of $\boldsymbol{H}\boldsymbol{H}^*$ and represent the attenuation

Transmit Power	10 W
Receive Power Range	0 dB - 90 dB
Receive Power Step Size	6 dB
Automatic Gain Control Range	40 dB - 112 dB
Automatic Gain Control Step Size	6 dB
Frequency Range	2 MHz - 70 MHz
Frequency Resolution	0.05 Hz
Group Delay Window	5 ms
Group Delay Resolution	0.02 ms
Sweep Rate	250 kHz/s, 500 kHz/s

Table 4.1. LLISP network specifications

of each eigenmode, and γ_i are the eigenvalues of $\boldsymbol{R}_{ss}$ and represent the power allocated to each eigenmode.

The capacity equation with full CSI available at the transmitter (2.15) was found to be

$$C_{fullCSI} = \sum_{i=1}^{k} \log_2(\frac{\mu\lambda_i}{\sigma_n^2})$$

where μ can be obtained from the optimal power allocation equation (2.13)

$$\gamma_i = (\mu - \frac{\sigma_n^2}{\lambda_i})^+$$

by applying the total transmit power constraint (2.14)

$$\sum_{i=1}^{r} \gamma_i = P_T.$$

The capacity equation with no CSI available at the transmitter (2.17) was found to be

$$C_{noCSI} = \sum_{i=1}^{n_T} \log_2(1 + \frac{P_T}{\sigma_n^2 n_T}\lambda_i).$$

As noted in Section 2.2.3, if all eigenmodes are of the same quality, $\lambda_1 = \lambda_2 = \ldots = \lambda_n$, capacity with and without CSI is the same. Furthermore, as P_T/σ_n^2 increases, capacity with no CSI at the transmitter approaches capacity with full CSI at the transmitter, irrespective of the relative quality of each eigenmode.

Ionograms from the LLISP network are stored as two dimensional arrays indexed by frequency and time (group delay), with the array entries representing the receive SNRs[4] ρ_{Rx} at each point in frequency and time, since an automatic gain control algorithm used in the LLISP receiver keeps the noise floor just below the signal detection level. The signal power received across propagating mode i is given by the product of the LLISP transmitter power P_{Tx} and the propagating mode attenuation λ_i, so the receive SNR ρ_{Rx_i} is given by the equation

$$\rho_{Rx_i} = \frac{P_{Tx}\lambda_i}{\sigma_n^2}. \tag{4.1}$$

SNR measurement is discussed more thoroughly in Section 6.7.

The post-processed form[5] of the LLISP data prevents propagating mode correlation from being calculated, so *propagating mode correlation is assumed to be zero*. Under this assumption, the propagating modes represent the eigenmodes of the channel, and the rank of $\boldsymbol{H}$ is simply the number of propagating modes. Mode correlation causes capacity to fall through reduced $\boldsymbol{H}$ rank. In addition, coarse receive power step size and limited group delay resolution make it difficult to separate modes with similar group delay, so in general the detected number of propagating modes will be less than the actual number of propagating modes present. While the zero mode correlation assumption will cause capacity values to be overestimated, the inability to detect all modes present will cause capacity values to be underestimated. Furthermore, because each LLISP ionogram is recorded using a single transmit and receive antenna, antenna correlation cannot be taken into account. The issues identified with the LLISP data provided motivation to develop the MCR for HF data collection.

For each frequency bin of an ionogram, the group delay data is processed to determine the number of modes present, and the ρ_{Rx_i} of each mode. A group of consecutive group delay ρ_{Rx} values above zero are considered a single mode, with the overall ρ_{Rx_i} for the mode taken to be the maximum of the consecutive group delay ρ_{Rx} values. This approach to mode detection cannot separate modes with similar group delay and was taken due to coarse receive power step size and limited group delay resolution. A diagram outlining the steps performed for mode detection is shown in Figure 4.2.

[4]The receive SNRs are measured in a small bandwidth equal to the frequency resolution of spectral data representing group delay.

[5]The post-processed form of the LLISP data is generated by grouping the time series data of a complete HF band sweep into small data blocks, and performing spectral estimation on the data blocks. Ionogram processing is described in detail in Chapter 6.

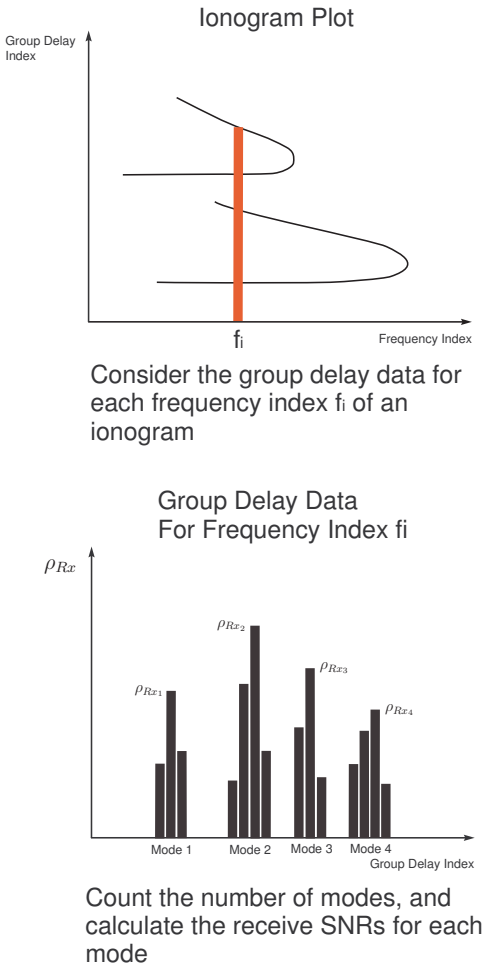

Figure 4.2. A diagram outlining the steps performed for mode detection

By inserting ρ_{Rx_i} and P_{Tx} values into (4.1), the term λ_i/σ_n^2 for each mode can be calculated, then inserted into (2.15) and (2.17) to give capacity for the full CSI and no CSI situations.

4.3 Results

The aim of the calculations is to determine the average capacity of a frequency hopping MIMO system for a typical HF transmit power constraint of P_T = 100 W, where only the best frequency bin of each ionogram, that is the frequency bin offering the highest capacity, is considered. In performing the calculations, the ionospheric data used was grouped according to transmitter, time period, and time of day. Data from two distinct periods was analysed, February 1996,

corresponding to a low T index[6], and February 2001, corresponding to a high T index. Day time was taken to be between 6:30 and 19:29.

For P_T = 100 W, full CSI and no CSI capacity equations were found to give approximately the same results. This is because capacity with no CSI at the transmitter approaches capacity with full CSI at the transmitter as P_T/σ_n^2 increases. The P_T/σ_n^2 term is large in our case because the small bandwidth SNR is measured in yields a small σ_n^2. For this reason, only the no CSI capacity results are presented here.

The results are presented in a series of tables and capacity histograms. Table 4.2 shows the number of ionogram samples used and the availability, which is the percentage of ionogram samples yielding non-zero capacities.

Table 4.3 shows average capacity C_{Ave}, the capacity uncertainty due to the 6 dB receive power step size ΔC_{Ave}, the average number of modes N_{Ave}, and the average time separation T_{Ave}. Average capacity uncertainty due to the 6 dB receive power step size was determined by adding/subtracting 3 dB to/from the receive SNRs and recalculating average capacity. The time separation is the maximum time separation between propagating modes, and this value is inversely proportional to the coherence bandwidth. The coherence bandwidth is the bandwidth over which the flat fading assumption holds, and represents an upper limit on the bandwidth[7] a spatial multiplexing system should use. Note that only samples yielding non-zero capacities were used to calculate the entries in Table 4.3.

Table 4.4 shows the maximum capacities encountered C_{Max}, and the corresponding number of modes N_{Max}, time separations T_{Max}, and capacity uncertainty due to the 6 dB receive power step size ΔC_{Max}.

Figures 4.3–4.9 show capacity histograms for each group of data, which give a detailed picture of capacity distribution. Note that only samples yielding non-zero capacities were used to generate these histograms.

From Table 4.3 we see that most average capacities were found to lie in the range of 40–90 bps/Hz. The corresponding average capacity uncertainty due to the 6 dB receive power step size was found to be approximately 1 bps/Hz per mode. From Table 4.4 we see that maximum capacities as high as 230 bps/Hz were calculated. Typical 100 W HF modems,

[6]The T index is an ionospheric index related to sunspot number which gives an indication of maximum usable frequency.

[7]In order to overcome this bandwidth limitation, spatial multiplexing can be combined with OFDM [75].

such as those that employ the Clover-2000 waveform developed by HAL communications, are designed to operate at a considerably lower spectral efficiency of around 0.25 bps/Hz in order to withstand significant multipath distortion [76]. It must be noted however that the Clover-2000 waveform employs 8 tones in a bandwidth of 2 MHz, so a direct comparison between the MIMO capacities calculated here for a small bandwidth equal to the frequency resolution of spectral data representing group delay, and Clover-2000 spectral efficiency, cannot be made.

As expected, higher capacities were achieved during day time of the high T index period, when the MUF (maximum usable frequency), and hence available HF bandwidth, is larger.

Figure 4.10 shows the ionogram that yielded the highest calculated capacity. This high capacity is due to the presence of a large number of modes at a frequency of around 5 MHz.

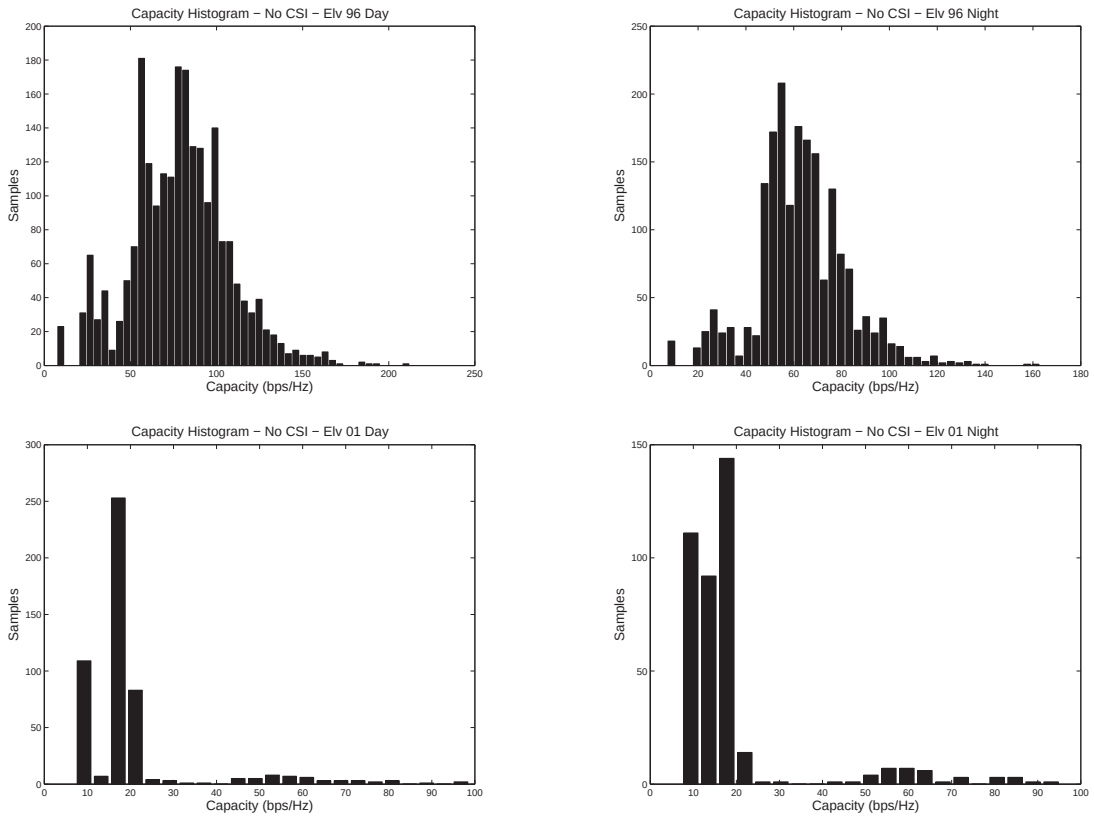

Figure 4.3. Capacity histograms for the Eleven Mile transmitter

Tx	Period	Day/Night	Number of Samples	Availability
Eleven Mile	96	Day	2,256	98%
Eleven Mile	96	Night	1,907	98%
Eleven Mile	01	Day	964	52.8%
Eleven Mile	01	Night	812	49.4%
Saipan	96	Day	1,502	66.4%
Saipan	96	Night	1,274	58.6%
Vanimo	96	Day	751	92.7%
Vanimo	96	Night	637	91.4%
Vanimo	01	Day	974	99.9%
Vanimo	01	Night	825	100%
Manila	96	Day	752	97.5%
Manila	96	Night	635	96.1%
Manila	01	Day	440	99.8%
Manila	01	Night	411	98.8%
Tennant Creek	96	Day	752	97.9%
Tennant Creek	96	Night	634	99.4%
Tennant Creek	01	Day	965	100%
Tennant Creek	01	Night	818	100%
Cocos Keeling	96	Day	748	73%
Cocos Keeling	96	Night	632	73.6%
Cocos Keeling	01	Day	987	99.7%
Cocos Keeling	01	Night	825	99.4%
Townsville	96	Day	750	49.2%
Townsville	96	Night	635	44.4%
Townsville	01	Day	965	99.5%
Townsville	01	Night	822	99.8%

Table 4.2. Number of samples and availability

4.4 Summary

HF MIMO capacities were calculated using data from the LLISP network of ionosondes under the idealistic assumption that propagating modes are uncorrelated. Most average HF MIMO capacities calculated were found to lie in the range of 40-90 bps/Hz. A number of issues were identified with the LLISP data, including the post processed form of the data which prevented propagating mode correlation from being calculated, and the coarse receive power step size and limited group delay resolution, which made it difficult to separate modes with similar group delay. The promising indicative capacity results obtained, coupled with the issues identified with

Tx	**Period**	**Day/Night**	C_{Ave} (bps/Hz)	ΔC_{Ave} (bps/Hz)	N_{Ave}	T_{Ave} (ms)
Eleven Mile	96	Day	77	3	3.04	1.8
Eleven Mile	96	Night	61	3	2.65	1.59
Eleven Mile	01	Day	18	1	1.14	0.24
Eleven Mile	01	Night	17	1	1.18	0.3
Saipan	96	Day	48	2	2.09	0.66
Saipan	96	Night	41	2	1.99	0.41
Vanimo	96	Day	90	4	3.69	1.44
Vanimo	96	Night	78	4	3.76	1.4
Vanimo	01	Day	108	4	4.38	2.29
Vanimo	01	Night	81	4	4.17	2.18
Manila	96	Day	72	3	2.99	0.9
Manila	96	Night	64	3	2.96	0.82
Manila	01	Day	85	4	3.57	1.58
Manila	01	Night	65	3	3.43	1.41
Tennant Creek	96	Day	54	2	2.08	0.66
Tennant Creek	96	Night	71	3	3.09	1.15
Tennant Creek	01	Day	93	4	3.75	2.07
Tennant Creek	01	Night	90	4	4.5	2.35
Cocos Keeling	96	Day	59	2	2.48	0.67
Cocos Keeling	96	Night	46	2	2.07	0.48
Cocos Keeling	01	Day	96	4	3.95	2.26
Cocos Keeling	01	Night	71	4	3.57	1.78
Townsville	96	Day	40	2	1.81	0.44
Townsville	96	Night	40	2	1.96	0.45
Townsville	01	Day	70	3	2.94	1.19
Townsville	01	Night	48	2	2.5	0.92

Table 4.3. Average capacity results for P_T = 100 W

the LLISP data, provided motivation for the development of the MCR for HF data collection, and for the continued investigation into HF MIMO capacity.

Tx	Period	Day/Night	C_{Max} (bps/Hz)	ΔC_{Max} (bps/Hz)	N_{Max}	T_{Max} (ms)
Elv	96	Day	210	10	10	4.1
Elv	96	Night	161	7	7	2.82
Elv	01	Day	97	5	5	1.66
Elv	01	Night	93	4	4	2.04
Sai	96	Day	156	6	6	3.4
Sai	96	Night	97	5	5	1.24
Van	96	Day	202	8	8	1.64
Van	96	Night	158	8	8	3.04
Van	01	Day	233	9	9	2.46
Van	01	Night	212	8	8	2.26
Man	96	Day	154	6	6	2.52
Man	96	Night	149	7	7	1.34
Man	01	Day	152	6	6	2.18
Man	01	Night	114	6	6	3.14
Ten	96	Day	144	6	6	3.08
Ten	96	Night	138	6	6	1.76
Ten	01	Day	186	8	8	2.34
Ten	01	Night	186	8	8	3.26
Coc	96	Day	157	7	7	1.88
Coc	96	Night	105	4	4	1.18
Coc	01	Day	188	8	8	2.42
Coc	01	Night	159	7	7	2.16
Tow	96	Day	117	5	5	2.38
Tow	96	Night	99	4	4	0.74
Tow	01	Day	182	8	8	3.22
Tow	01	Night	127	5	5	1.04

Table 4.4. Maximum capacity results for P_T = 100 W

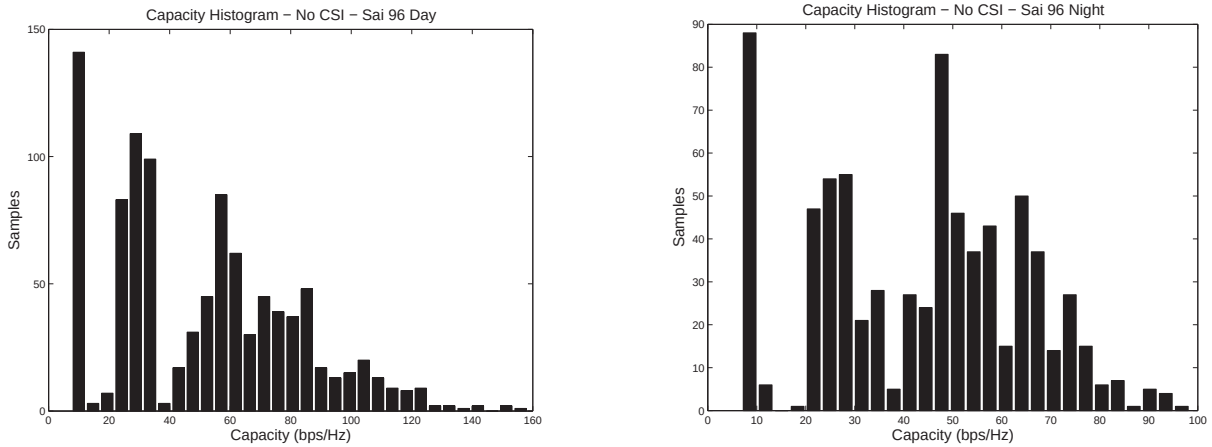

Figure 4.4. Capacity histograms for the Saipan transmitter

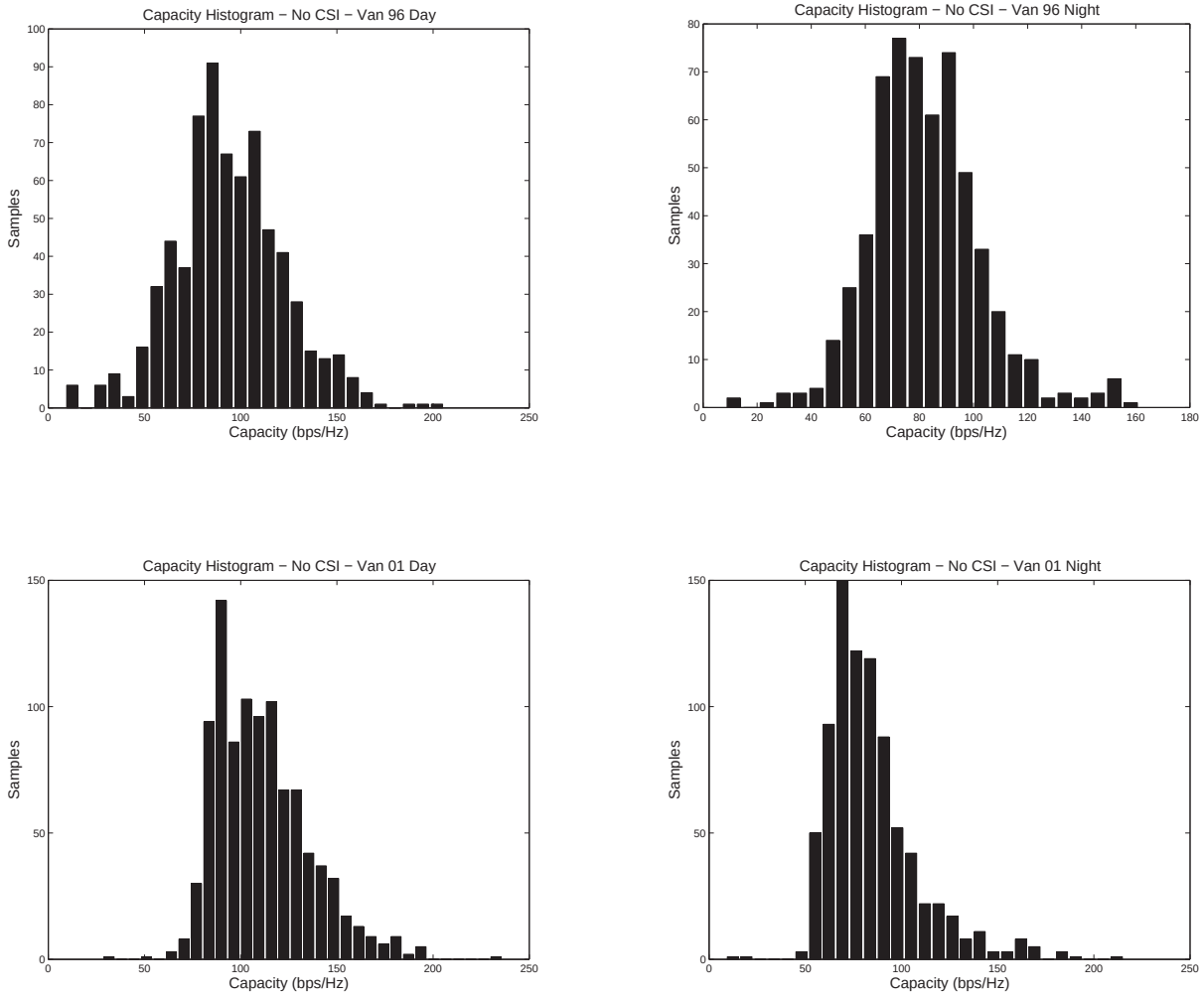

Figure 4.5. Capacity histograms for the Vanimo transmitter

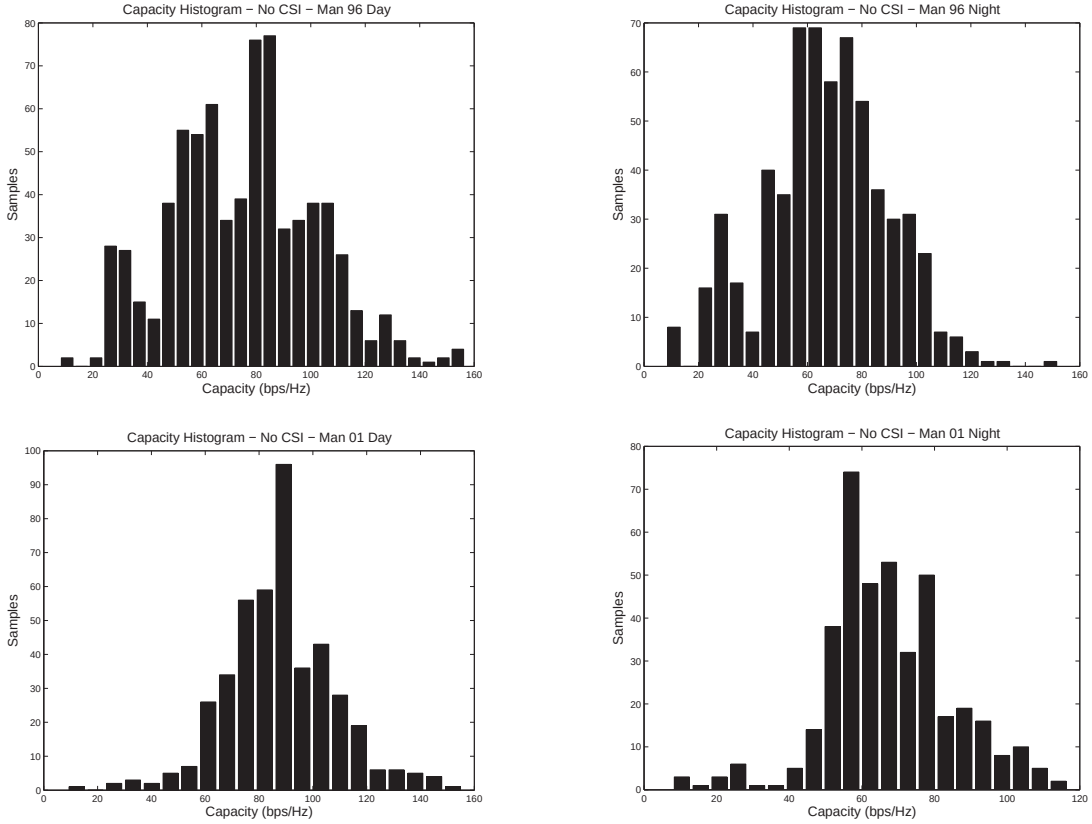

Figure 4.6. Capacity histograms for the Manila transmitter

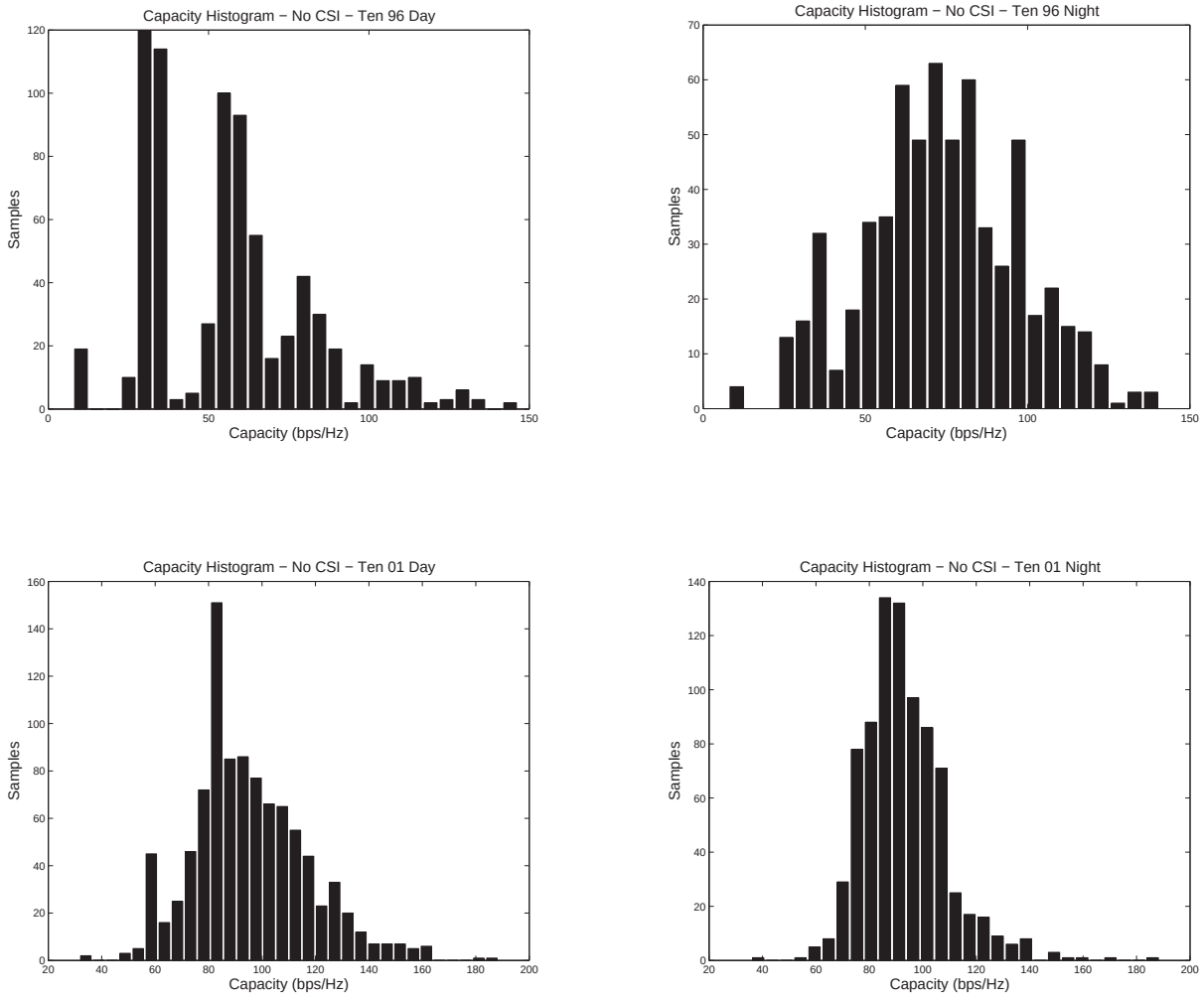

Figure 4.7. Capacity histograms for the Tennant Creek transmitter

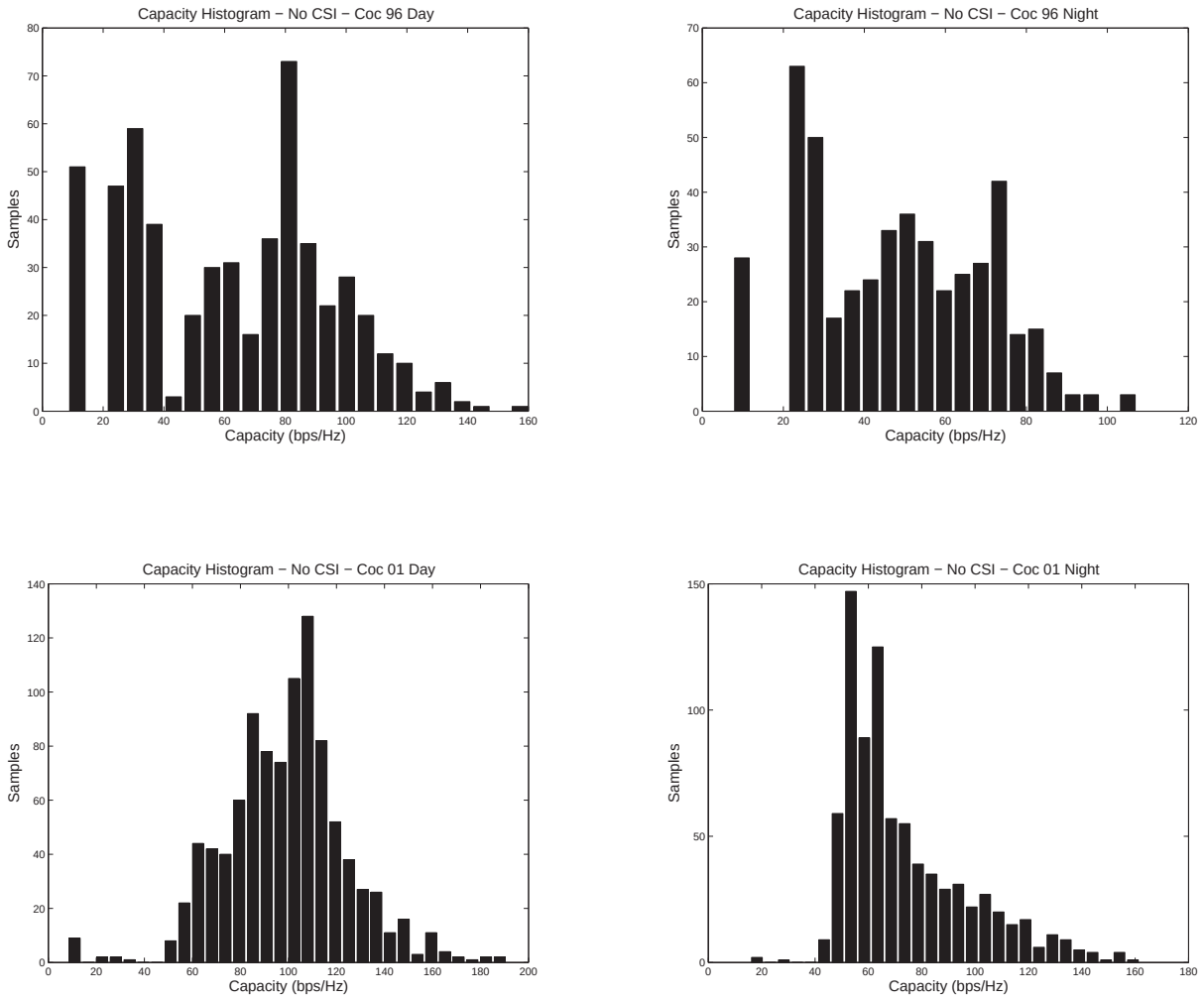

Figure 4.8. Capacity histograms for the Cocos Keeling transmitter

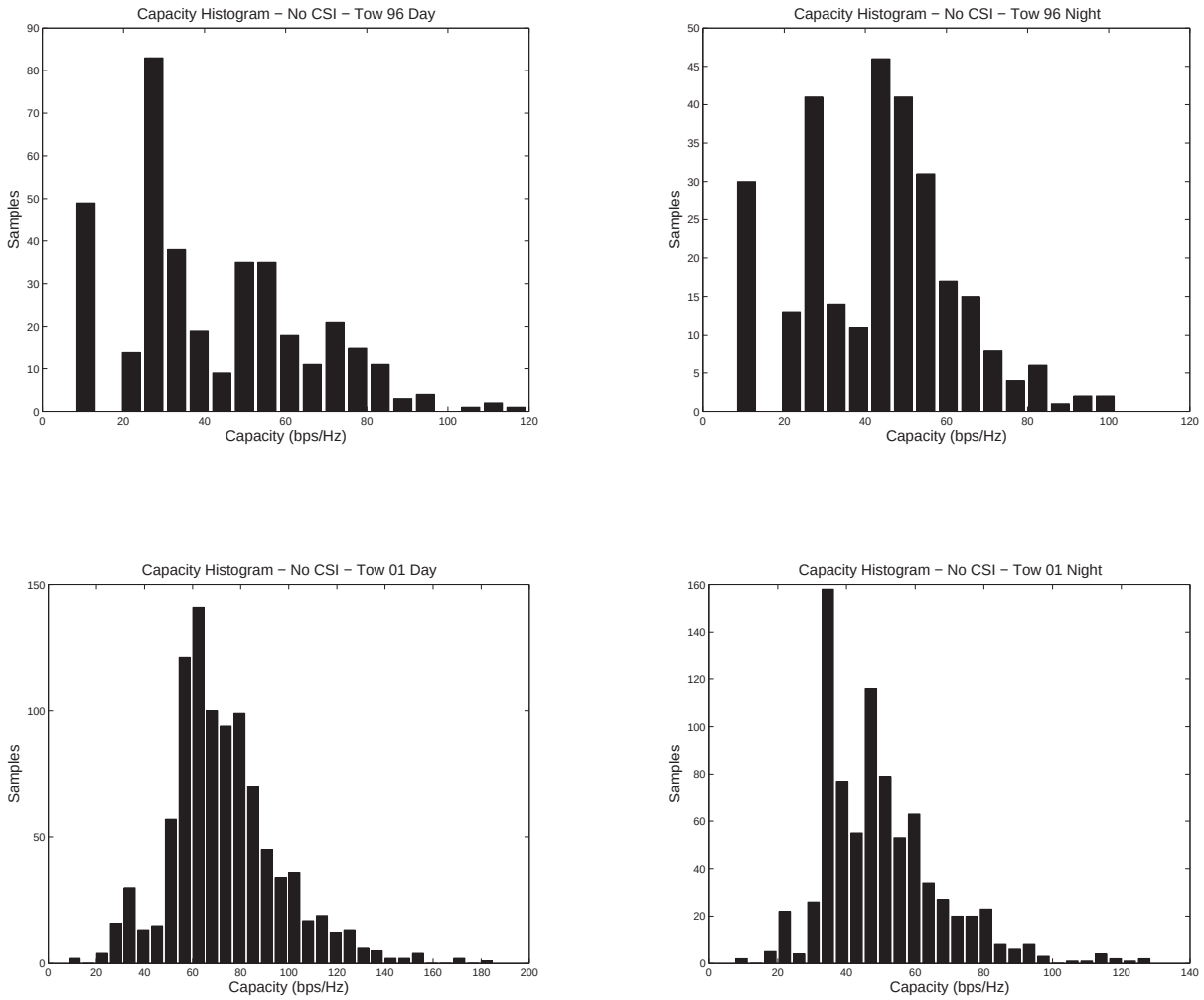

Figure 4.9. Capacity histograms for the Townsville transmitter

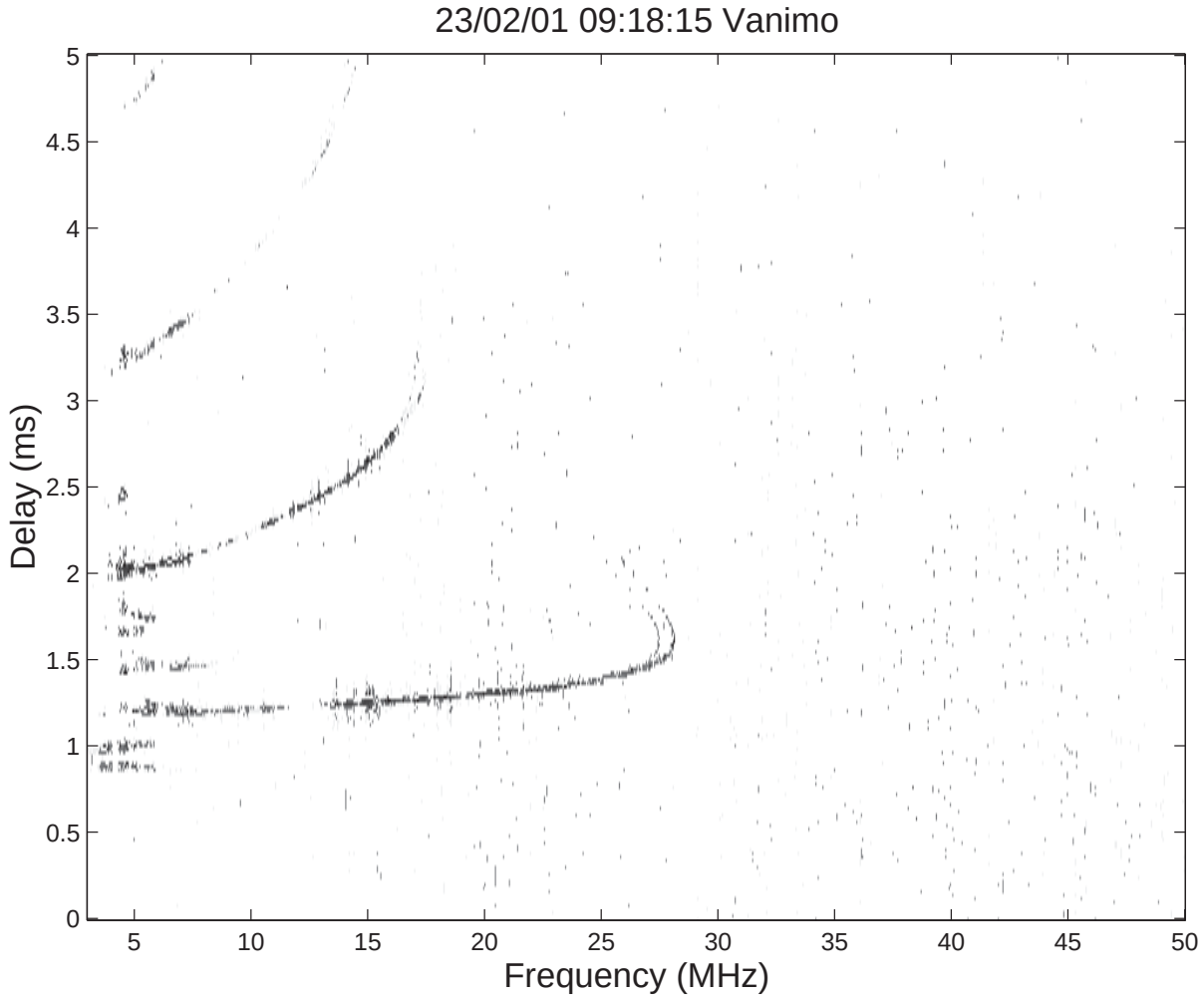

Figure 4.10. Ionogram yielding the highest calculated capacity

Chapter 5

HF MIMO Theory

In the previous chapter HF MIMO capacity was calculated from existing ionosonde data. The positive results obtained, coupled with the issues identified with the ionosonde data, provided motivation to continue the investigation into HF MIMO capacity. The next step taken in the investigation was to determine the structure of the HF MIMO channel matrix. A model for the structure of the HF MIMO channel matrix was developed according to the signal paths and gains between transmit and receive antenna array elements communicating in the HF band via ionospheric propagation. This model gives an insight into the factors limiting HF MIMO capacity, such as the number of receive antennas n_R, the number of transmit antennas n_T, the number of propagating modes m, and the amount of receive antenna correlation, transmit antenna correlation, and propagating mode correlation present. The rank properties of channel matrices given by the HF MIMO channel matrix model were found to be the same as channel matrices given by the Gesbert MIMO channel model [27], as antenna and mode correlation was varied. This finding indicated that HF MIMO capacity could be calculated by measuring antenna and mode correlation matrices, substituting the correlation matrices into the Gesbert MIMO channel model to generate channel matrices, and then substituting the generated channel matrices into the general MIMO capacity equation (2.8) to yield capacity. The advantage of this approach is that the system required to record data for calculation of correlation matrices is significantly less complex compared to the system required to record the channel matrix directly. Measuring mode correlation requires only a single transmit and receive antenna, while measuring antenna correlation requires a single transmit antenna, and a small number of receive antenna elements. Measuring the channel matrix directly on the other hand requires a large number of transmit and receive antenna elements, and the number of antenna elements

used places an upper limit on the rank, and hence capacity, of the recorded channel matrices. The following subsections detail the HF MIMO channel matrix model, and the generation of channel matrices from correlation data.

5.1 HF MIMO Channel Matrix Model

Figure 5.1 shows a diagram of an HF MIMO system with n_T transmit antennas, m propagating modes, and n_R receive antennas. The diagram is redrawn in Figure 5.2 to show the different paths present between the n_T transmit antennas and n_R receive antennas when m modes are present, under the assumption that array elements are closely spaced, such that each transmit-receive antenna pair shares approximately the same propagating modes. The common gain between transmit-receive antenna pairs over a particular propagating mode can be attributed to the propagating mode gain. The differences in gains between transmit-receive antenna pairs can be attributed to the differences in spatial location of the antenna elements, and accounted for by introducing gain factors for the propagation between the receive antennas and the propagating modes, as well as gain factors for the propagation between the propagating modes and the transmit antennas. Figure 5.3 shows simultaneous ionograms recorded from antennas 1 and 3 of the antenna array given in Figure 6.2, and their similarity supports the assumption that each transmit-receive antenna pair shares approximately the same propagating modes when antenna elements are closely spaced.

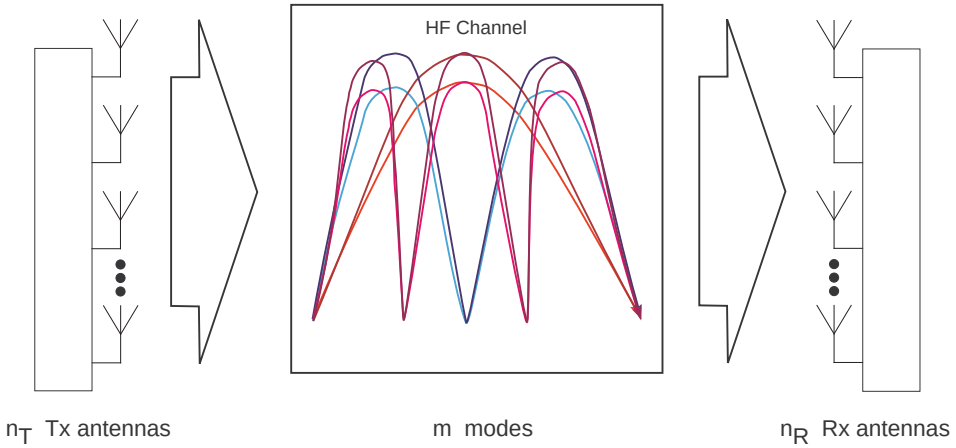

Figure 5.1. Diagram of an HF MIMO system

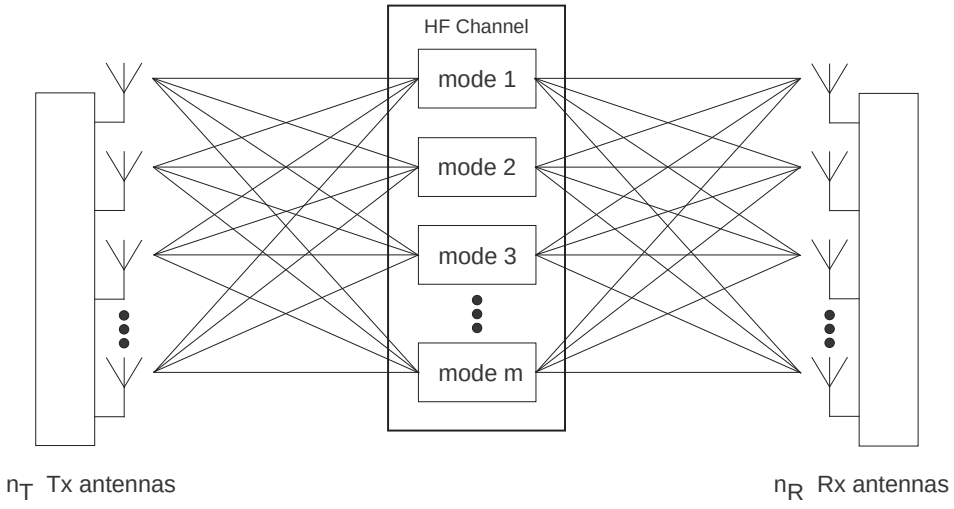

Figure 5.2. Signal paths in an HF MIMO system when transmit and receive antenna elements are closely spaced

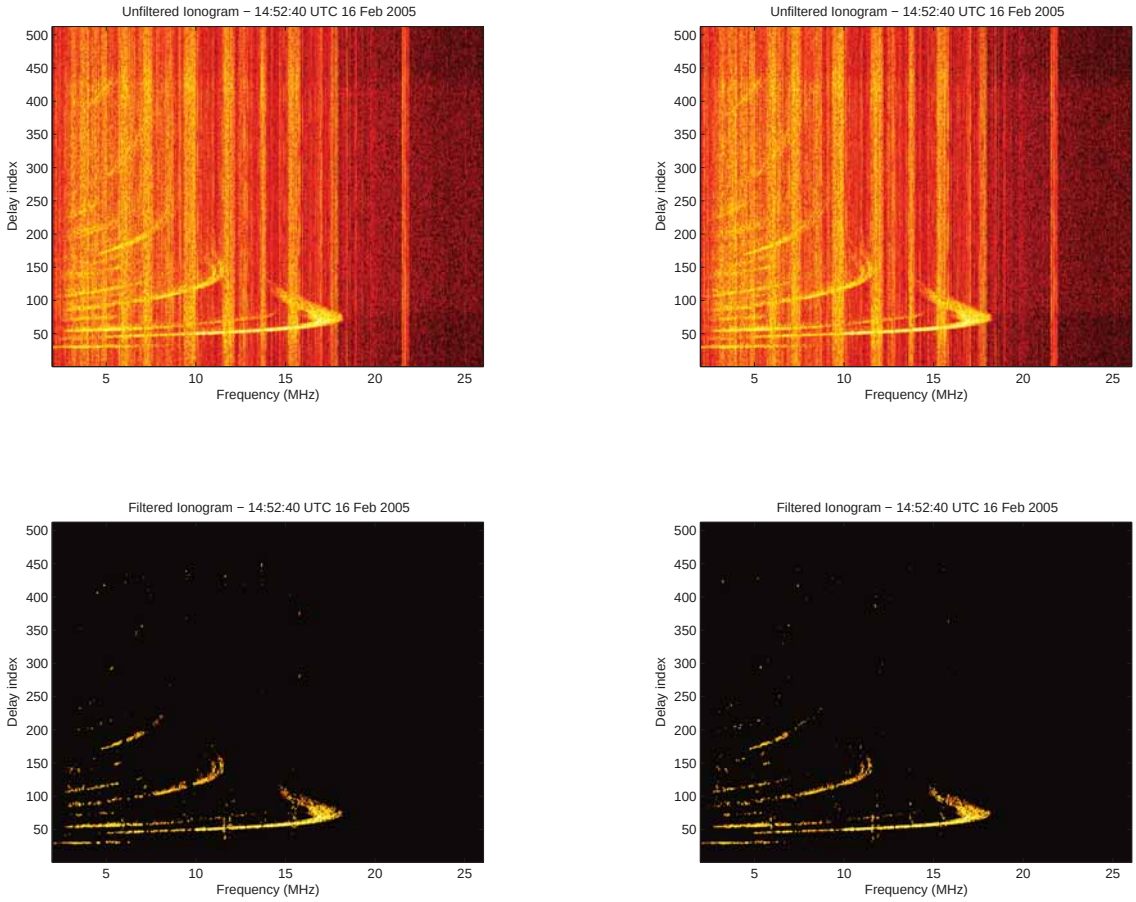

Figure 5.3. Ionograms recorded simultaneously from two closely spaced antennas appear to be very similar and thus the antennas share approximately the same propagating modes

From Figure 5.2 we see that the channel matrix can be written as

$$\boldsymbol{H} = \begin{bmatrix} g_{1,1,1}+g_{1,2,1}+\cdots+g_{1,m,1} & g_{1,1,2}+g_{1,2,2}+\cdots+g_{1,m,2} & \cdots & \\ g_{2,1,1}+g_{2,2,1}+\cdots+g_{2,m,1} & g_{2,1,2}+g_{2,2,2}+\cdots+g_{2,m,2} & \cdots & \\ \vdots & \vdots & \ddots & \\ & & & g_{n_R,1,n_T}+g_{n_R,2,n_T}+\cdots+g_{n_R,m,n_T} \end{bmatrix} \tag{5.1}$$

where $g_{i,j,k}$ is the complex transfer function between transmit antenna k and receive antenna i through mode j. Equivalently, the channel matrix can be written as a product of three matrices $\boldsymbol{R} \in \mathbb{C}^{n_R \times m}$, $\boldsymbol{M} \in \mathbb{C}^{m \times m}$ and $\boldsymbol{T} \in \mathbb{C}^{m \times n_T}$ to give

$$\boldsymbol{H} = \boldsymbol{R}\,\boldsymbol{M}\,\boldsymbol{T}$$

where

$$\boldsymbol{R} = \begin{bmatrix} g_{rm_{1,1}} & g_{rm_{1,2}} & \cdots & g_{rm_{1,m}} \\ g_{rm_{2,1}} & g_{rm_{2,2}} & \cdots & g_{rm_{2,m}} \\ \vdots & \vdots & \ddots & \vdots \\ g_{rm_{n_R,1}} & g_{rm_{n_R,2}} & \cdots & g_{rm_{n_R,m}} \end{bmatrix}$$

$$\boldsymbol{M} = \begin{bmatrix} g_{m_1} & 0 & \ldots & 0 \\ 0 & g_{m_2} & & 0 \\ \vdots & & \ddots & \vdots \\ 0 & 0 & \ldots & g_{m_m} \end{bmatrix}$$

$$\boldsymbol{T} = \begin{bmatrix} g_{mt_{1,1}} & g_{mt_{1,2}} & \cdots & g_{mt_{1,n_T}} \\ g_{mt_{2,1}} & g_{mt_{2,2}} & \cdots & g_{mt_{2,n_T}} \\ \vdots & \vdots & \ddots & \vdots \\ g_{mt_{m,1}} & g_{mt_{m,2}} & \cdots & g_{mt_{m,n_T}} \end{bmatrix}$$

and

$$g_{i,j,k} = g_{rm_{i,j}}\; g_{m_j}\; g_{mt_{j,k}}.$$

Here $\boldsymbol{R}$ is the receive antenna-propagating mode matrix comprising elements $g_{rm_{i,j}}$ which represent the complex transfer function between receive antenna i and mode j, $\boldsymbol{M}$ is the propagating mode matrix comprising elements g_{m_i} which represent the complex transfer function of mode i, and $\boldsymbol{T}$ is the propagating mode-transmit antenna matrix comprising elements $g_{mt_{i,j}}$

which represent the complex transfer function between mode i and transmit antenna j. The impact of antenna and mode correlation is considered in the following subsections.

5.1.1 Receive Antenna Correlation

Consider the situation where the n_R receive antennas are fully correlated, whilst the m propagating modes and n_T transmit antennas are fully uncorrelated. In this case the transfer functions between all receive antennas and a particular mode are the same

$$g_{rm_{1,j}} = g_{rm_{2,j}} = \ldots = g_{rm_{n_R,j}}.$$

Setting $g_{rm_{i,j}} \equiv g_{rm_{1,j}}$, the receive antenna-propagating mode matrix $\boldsymbol{R}$ becomes a rank 1 matrix with each row the same

$$\boldsymbol{R} = \begin{bmatrix} g_{rm_{1,1}} & g_{rm_{1,2}} & \cdots & g_{rm_{1,m}} \\ g_{rm_{1,1}} & g_{rm_{1,2}} & \cdots & g_{rm_{1,m}} \\ \vdots & \vdots & \ddots & \vdots \\ g_{rm_{1,1}} & g_{rm_{1,2}} & \cdots & g_{rm_{1,m}} \end{bmatrix}.$$

Setting $g_{i,j,k} = g_{rm_{i,j}}\, g_{m_j}\, g_{mt_{j,k}} \equiv g_{rm_{1,j}}\, g_{m_j}\, g_{mt_{j,k}} \equiv g_{1,j,k}$, the channel matrix becomes a rank 1 matrix with each row the same

$$\boldsymbol{H} = \begin{bmatrix} g_{1,1,1} + g_{1,2,1} + \ldots + g_{1,m,1} & g_{1,1,2} + g_{1,2,2} + \ldots + g_{1,m,2} & \cdots \\ g_{1,1,1} + g_{1,2,1} + \ldots + g_{1,m,1} & g_{1,1,2} + g_{1,2,2} + \ldots + g_{1,m,2} & \cdots \\ \vdots & \vdots & \ddots \end{bmatrix}.$$

5.1.2 Transmit Antenna Correlation

Consider the situation where the n_T transmit antennas are fully correlated, whilst the m propagating modes and n_R receive antennas are fully uncorrelated. In this case the transfer functions between all transmit antennas and a particular mode are the same

$$g_{mt_{j,1}} = g_{mt_{j,2}} = \ldots = g_{mt_{j,n_T}}.$$

Setting $g_{mt_{j,k}} \equiv g_{mt_{j,1}}$, the transmit antenna-propagating mode matrix $\boldsymbol{T}$ becomes a rank 1 matrix with each column the same

$$\boldsymbol{T} = \begin{bmatrix} g_{mt_{1,1}} & g_{mt_{1,1}} & \cdots & g_{mt_{1,1}} \\ g_{mt_{2,1}} & g_{mt_{2,1}} & \cdots & g_{mt_{2,1}} \\ \vdots & \vdots & \ddots & \vdots \\ g_{mt_{m,1}} & g_{mt_{m,1}} & \cdots & g_{mt_{m,1}} \end{bmatrix}.$$

Setting $g_{i,j,k} = g_{rm_{i,j}}\, g_{m_j}\, g_{mt_{j,k}} \equiv g_{rm_{i,j}}\, g_{m_j}\, g_{mt_{j,1}} \equiv g_{i,j,1}$, the channel matrix becomes a rank 1 matrix with each column the same

$$\boldsymbol{H} = \begin{bmatrix} g_{1,1,1} + g_{1,2,1} + \ldots + g_{1,m,1} & g_{1,1,1} + g_{1,2,1} + \ldots + g_{1,m,1} & \cdots \\ g_{2,1,1} + g_{2,2,1} + \ldots + g_{2,m,1} & g_{2,1,1} + g_{2,2,1} + \ldots + g_{2,m,1} & \cdots \\ \vdots & \vdots & \ddots \end{bmatrix}.$$

5.1.3 Propagating Mode Correlation

Consider the situation where the m propagating modes are fully correlated, whilst the n_T transmit antennas and n_R receive antennas are fully uncorrelated. In this case the propagating mode transfer functions are the same

$$g_{m_1} = g_{m_2} = \ldots = g_{m_j}.$$

In addition, the transfer functions between all propagating modes and a particular transmit antenna are the same

$$g_{mt_{1,k}} = g_{mt_{2,k}} = \ldots = g_{mt_{m,k}}$$

as are the transfer functions between all propagating modes and a particular receive antenna

$$g_{rm_{i,1}} = g_{rm_{i,2}} = \ldots = g_{rm_{i,m}}.$$

Setting $g_{i,j,k} = g_{rm_{i,j}}\ g_{m_j}\ g_{mt_{j,k}} \equiv g_{rm_{i,1}}\ g_{m_1}\ g_{mt_{1,k}} \equiv g_{i,1,k}$, the channel matrix becomes

$$
\begin{aligned}
\boldsymbol{H} &= \begin{bmatrix}
g_{1,1,1}+g_{1,1,1}+\ldots+g_{1,1,1} & g_{1,1,2}+g_{1,1,2}+\ldots+g_{1,1,2} & \cdots & \\
g_{2,1,1}+g_{2,1,1}+\ldots+g_{2,1,1} & g_{2,1,2}+g_{2,1,2}+\ldots+g_{2,1,2} & \cdots & \\
\vdots & \vdots & \ddots & \\
 & & & g_{n_R,1,n_T}+g_{n_R,1,n_T}+\ldots+g_{n_R,1,n_T}
\end{bmatrix} \\
&= m \begin{bmatrix}
g_{1,1,1} & g_{1,1,2} & \cdots & \\
g_{2,1,1} & g_{2,1,2} & \cdots & \\
\vdots & \vdots & \ddots & \\
 & & & g_{n_R,1,n_T}
\end{bmatrix} \\
&= m\ g_{m_1} \begin{bmatrix}
g_{rm_{1,1}}g_{mt_{1,1}} & g_{rm_{1,1}}g_{mt_{1,2}} & \cdots & \\
g_{rm_{2,1}}g_{mt_{1,1}} & g_{rm_{2,1}}g_{mt_{1,2}} & \cdots & \\
\vdots & \vdots & \ddots & \\
 & & & g_{rm_{n_R,1}}g_{mt_{1,n_T}}
\end{bmatrix}.
\end{aligned}
$$

Note that $\boldsymbol{H}_{i.} = \frac{g_{rm_{1,1}}}{g_{rm_{i,1}}}\ \boldsymbol{H}_{1.}$, where $\boldsymbol{H}_{i.}$ refers to row i of $\boldsymbol{H}$. Thus $\boldsymbol{H}$ has a single linearly independent row, and is rank 1, even though the channel matrix elements are in fact uncorrelated. Such a channel is referred to as a *keyhole* [37].

5.1.4 HF MIMO Channel Matrix Model When Antennas are not Closely Spaced

The HF MIMO channel matrix model (5.1) is valid for the common scenario where transmit and receive antenna array elements are closely spaced, and each pair of transmit and receive antennas shares approximately the same propagating modes. For such a scenario, the channel matrix can be conveniently factored into a product of three matrices, and maximum channel matrix rank is dependent on the number of propagating modes m, and correlation between the modes. When transmit and receive antenna array elements are not closely spaced, the structure of the channel matrix will become more complex, and the rank of the channel matrix will generally be higher, leading to higher capacities. Two distinct situations are considered in the following subsections.

HF MIMO Channel Matrix When Transmit Antenna Elements are Widely Spaced and Receive Antenna Elements are Closely Spaced

Consider the situation where the transmit antenna elements are widely spaced, and the receive antenna elements are closely spaced. For instance the transmit array could be located on a large vacant area of land where the transmit elements can be spread out a long distance apart, while the receive array could be located on a ship where the receive elements are forced to be close together. In such a situation, signals from each transmit antenna will propagate over a distinctly different set of propagating modes, and the number of propagating modes available for each transmit antenna is likely to be different. Figure 5.4 shows the signal paths for this situation. Observe the ionograms shown in Figures 7.8-7.11 of Chapter 7. The ionograms shown are captured a matter of seconds apart, while the antennas are reportedly located at the same site. The difference in time can't account for such a marked difference between the ionograms, so the spatial difference between the transmit elements is likely to be a major cause. It would be useful to determine the antenna spacings for which this behaviour is observed, however the spacing of the remote transmitters is not known.

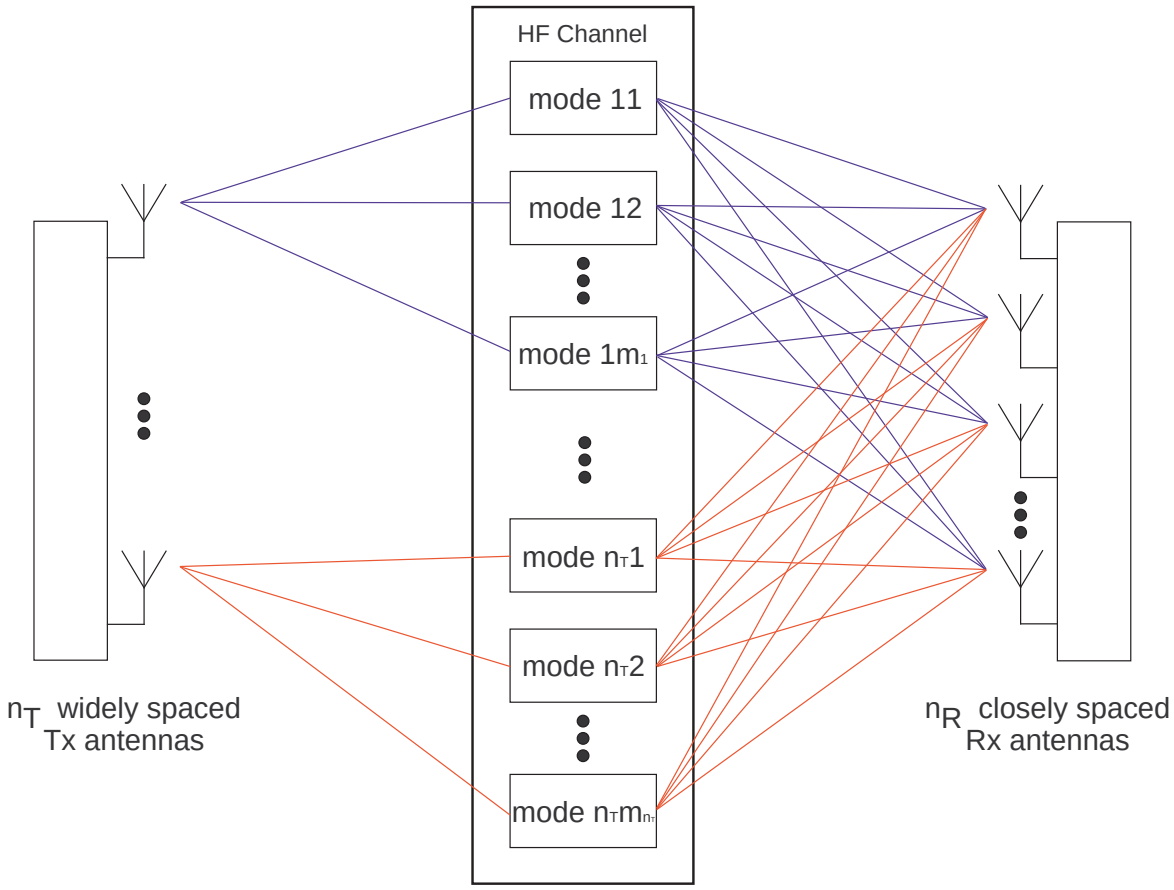

Figure 5.4. Signal paths in an HF MIMO system when transmit antenna elements are widely spaced and receive antenna elements are closely spaced

From Figure 5.4 we see that the channel matrix can be written as

$$\boldsymbol{H} = \begin{bmatrix} g_{1,11,1} + g_{1,12,1} + \ldots + g_{1,1m_1,1} & \cdots & \\ g_{2,11,1} + g_{2,12,1} + \ldots + g_{2,1m_1,1} & \cdots & \\ \vdots & \ddots & \\ & & g_{n_R,n_T1,n_T} + g_{n_R,n_T2,n_T} + \ldots + g_{n_R,n_Tm_{n_T},n_T} \end{bmatrix}$$

where $g_{i,kj,k}$ is the complex transfer function between transmit antenna k and receive antenna i through mode kj, mode kj is the jth mode of the set of modes for transmit antenna k, and m_k is the number of modes for transmit antenna k.

Equivalently, the channel matrix can be written in the form

$$\boldsymbol{H} = \begin{bmatrix} \boldsymbol{T_1} & \boldsymbol{T_2} & \dots & \boldsymbol{T_{n_T}} \end{bmatrix}$$

where

$$\boldsymbol{T_k} = \begin{bmatrix} g_{rm_{1,k1}} & g_{rm_{1,k2}} & \cdots & g_{rm_{1,km_k}} \\ g_{rm_{2,k1}} & g_{rm_{2,k2}} & \cdots & g_{rm_{2,km_k}} \\ \vdots & \vdots & \ddots & \vdots \\ g_{rm_{n_R,k1}} & g_{rm_{n_R,k2}} & \cdots & g_{rm_{n_R,km_k}} \end{bmatrix} \begin{bmatrix} g_{m_{k1}} g_{mt_{k1,k}} \\ g_{m_{k2}} g_{mt_{k2,k}} \\ \vdots \\ g_{m_{km_k}} g_{mt_{km_k,k}} \end{bmatrix}$$

and

$$g_{i,kj,k} = g_{rm_{i,kj}}\, g_{m_{kj}}\, g_{mt_{kj,k}}.$$

HF MIMO Channel Matrix When Transmit and Receive Antenna Elements are Both Widely Spaced

If both transmit antenna elements and receive antenna elements are widely spaced, the gains between each transmit-receive antenna pair will be uncorrelated, and channel matrix rank will not be limited by the number of propagating modes m, nor the propagating mode correlation. For this situation the Rayleigh channel model is an appropriate model for the channel matrix.

5.1.5 Summary

To summarize, the following observations can be made about the rank properties of the channel matrix for different antenna and mode correlation conditions when transmit and receive antenna elements are closely spaced

- The presence of either full receive antenna correlation, full transmit antenna correlation, or full mode correlation will yield a rank 1 channel matrix.

- If receive antennas, transmit antennas and modes are fully uncorrelated, the channel matrix is full rank, with rank value given by the minimum of n_T, n_R, and m.

- Maximum channel matrix rank is dependent on the number of propagating modes m, and correlation between propagating modes. This is because we have control over the design of the transmit and receive antenna arrays.
- Given m uncorrelated propagating modes we should use m uncorrelated transmit and m uncorrelated receive antennas to achieve the maximum channel matrix rank of m. If some transmit and receive antenna correlation exists, we require $n_T, n_R > m$ to achieve a maximum rank channel matrix.

As transmit and receive antenna element spacing is increased, the structure of the channel matrix becomes more complex, and channel matrix rank increases accordingly. With large antenna element spacing at both the transmit and receive ends, the channel matrix is not limited by the number of propagating modes m, nor the propagating mode correlation. For such a case the channel matrix may be modelled using the Rayleigh channel model.

5.2 Channel Matrix Generation Using Correlation Data

In the previous section we saw that the rank of the HF channel matrix is not just a function of the number of receive antennas n_R, the number of transmit antennas n_T, and the number of propagating modes m, but also of the amount of receive antenna correlation, transmit antenna correlation, and propagating mode correlation present. In this section we show that a channel matrix can be generated from receive antenna correlation, transmit correlation, and mode correlation matrices. The generated channel matrix is shown to possess the same rank properties as the channel matrix given by the HF channel matrix model (5.1), as antenna and mode correlation is varied. This means that measuring antenna correlation and mode correlation matrices, and using these matrices to generate a channel matrix, is a possible alternative to measuring the channel matrix directly, for the purposes of capacity calculations. The advantage of such an approach is that the system required to record data for calculation of correlation matrices is significantly less complex compared to the system required to record the channel matrix directly. Measuring mode correlation requires only a single transmit and receive antenna, while measuring antenna correlation requires a single transmit antenna, and a small number of receive antenna elements. Measuring the channel matrix directly on the other hand requires a large number of transmit and receive antenna elements, and the number of antenna elements used places an upper limit on the rank, and hence capacity, of the recorded channel matrices.

A correlation matrix $\boldsymbol{C} \in \mathbb{R}^{n \times n}$ is of the form

$$\boldsymbol{C} = (c_{ij}) = \begin{bmatrix} 1 & c_{12} & \dots & c_{1n} \\ c_{21} & 1 & \dots & c_{2n} \\ \vdots & \vdots & \ddots & \vdots \\ c_{n1} & c_{n2} & \dots & 1 \end{bmatrix}$$

where c_{ij} is the correlation between the variable with index i and the variable with index j. The diagonal of the correlation matrix comprises of 1s, since the correlation of a variable with itself is always 1. The correlation matrix is symmetric about the diagonal since $c_{ij} = c_{ji}$.

Given a transmit antenna correlation matrix $\boldsymbol{C}_t \in \mathbb{R}^{n_T \times n_T}$, a receive antenna correlation matrix $\boldsymbol{C}_r \in \mathbb{R}^{n_R \times n_R}$, and a mode correlation matrix $\boldsymbol{C}_m \in \mathbb{R}^{m \times m}$, the Gesbert MIMO channel model [27] yields a channel matrix given by

$$\boldsymbol{H} = \frac{1}{\sqrt{m}} (\boldsymbol{C}_r)^{\frac{1}{2}} \boldsymbol{G}_{rm} (\boldsymbol{C}_m)^{\frac{1}{2}} \boldsymbol{G}_{mt} (\boldsymbol{C}_t)^{\frac{1}{2}} \tag{5.2}$$

where $\boldsymbol{G}_{rm} \in \mathbb{C}^{n_R \times m}$ and $\boldsymbol{G}_{mt} \in \mathbb{C}^{m \times n_T}$ contain iid circularly symmetric zero mean unit variance complex Gaussian entries as given by the Rayleigh channel model. The scaling factor $1/\sqrt{m}$ normalizes the channel energy such that it is independent of the number of modes, $||\boldsymbol{H}||_F^2 = n_R \, n_T$, compared with $||\boldsymbol{H}||_F^2 = n_R \, m \, n_T$ in the absence of the scaling factor. Note that the Gesbert MIMO channel model is a modified version of the Kronecker MIMO channel model that assumes correlation matrices are separable [77]. The Weichselberger channel model is an alternate to the Kronecker model that takes into account coupling between transmit and receive arrays [78].

The behaviour of the Gesbert model for different correlation situations can be demonstrated by setting the correlation matrices $\boldsymbol{C}_t, \boldsymbol{C}_r$, and $\boldsymbol{C}_m$ to either the identity matrix for full decorrelation, or the all 1s matrix for full correlation. Before we do this it is useful to observe the effect of multiplying an $n \times n$ matrix $\boldsymbol{A}_n$ (which could comprise of either real or complex elements)

by the all 1s matrix $\boldsymbol{J}_n \in \mathbb{R}^{n\times n}$

$$\begin{aligned}\boldsymbol{J}_n\boldsymbol{A}_n &= \begin{bmatrix} 1 & 1 & \dots & 1 \\ 1 & 1 & \dots & 1 \\ \vdots & \vdots & \ddots & \vdots \\ 1 & 1 & \dots & 1 \end{bmatrix} \begin{bmatrix} a_{11} & a_{12} & \dots & a_{1n} \\ a_{21} & a_{22} & \dots & a_{2n} \\ \vdots & \vdots & \ddots & \vdots \\ a_{n1} & a_{n2} & \dots & a_{nn} \end{bmatrix} \\ &= \begin{bmatrix} a_{11}+a_{21}+\ldots+a_{n1} & \dots & a_{1n}+a_{2n}+\ldots+a_{nn} \\ a_{11}+a_{21}+\ldots+a_{n1} & \dots & a_{1n}+a_{2n}+\ldots+a_{nn} \\ \vdots & \ddots & \vdots \\ a_{11}+a_{21}+\ldots+a_{n1} & \dots & a_{1n}+a_{2n}+\ldots+a_{nn} \end{bmatrix}. \end{aligned} \tag{5.3}$$

The resulting matrix has a single linearly independent row and is therefore rank 1. Similarly the matrix product $\boldsymbol{A}_n\boldsymbol{J}_n$ is also rank 1.

5.2.1 The Effect of Full Receive Antenna Correlation and Transmit Antenna Correlation on the Gesbert Model Channel Matrix

Consider the situation where the receive antennas are fully correlated, $\boldsymbol{C}_r = \boldsymbol{J}_{n_R}$, the transmit antennas are fully uncorrelated, $\boldsymbol{C}_t = \boldsymbol{I}_{n_T}$, and the propagating modes are fully uncorrelated, $\boldsymbol{C}_m = \boldsymbol{I}_m$. Substituting these values into (5.2) we get

$$\begin{aligned}\boldsymbol{H} &= \frac{1}{\sqrt{m}}(\boldsymbol{J}_{n_R})^{\frac{1}{2}}\boldsymbol{G}_{rm}(\boldsymbol{I}_m)^{\frac{1}{2}}\boldsymbol{G}_{mt}(\boldsymbol{I}_{n_T})^{\frac{1}{2}} \\ &= \frac{1}{\sqrt{m}}(\boldsymbol{J}_{n_R})^{\frac{1}{2}}\boldsymbol{G}_{rm}\boldsymbol{G}_{mt} \\ &= \frac{1}{\sqrt{n_R\, m}}\boldsymbol{J}_{n_R}\boldsymbol{G}_{rm}\boldsymbol{G}_{mt}.\end{aligned}$$

Using the property shown in (5.3), the channel matrix is rank 1. In the same way, it can be shown that full transmit antenna correlation will collapse channel matrix rank to 1. For the above situation also consider the elements g_{ij} of $\boldsymbol{J}_{n_R}\boldsymbol{G}_{rm}\boldsymbol{G}_{mt}$, which are given by

$$g_{ij} = g_{1j} = (g_{rm_{1,1}} + \ldots + g_{rm_{n_R,1}})g_{mt_{1,j}} + \ldots + (g_{rm_{1,m}} + \ldots + g_{rm_{n_R,m}})g_{mt_{m,j}}.$$

The g_{ij} are distributed as $\mathcal{CN}(0, n_R\, m)$, and the factor $1/\sqrt{n_R\, m}$ scales the distribution of the channel matrix entries to $\mathcal{CN}(0,1)$, yielding the desired normalized total channel energy of $||\boldsymbol{H}||_F^2 = n_R\, n_T$.

5.2.2 The Effect of Full Propagating Mode Correlation on the Gesbert Model Channel Matrix

Consider the situation where the receive antennas are fully uncorrelated, $\boldsymbol{C}_r = \boldsymbol{I}_{n_R}$, the transmit antennas are fully uncorrelated, $\boldsymbol{C}_t = \boldsymbol{I}_{n_T}$, and the propagating modes are fully correlated, $\boldsymbol{C}_m = \boldsymbol{J}_m$. Substituting these values into (5.2) we get

$$
\begin{aligned}
\boldsymbol{H} &= \frac{1}{\sqrt{m}}(\boldsymbol{I}_{n_R})^{\frac{1}{2}}\boldsymbol{G}_{rm}(\boldsymbol{J}_m)^{\frac{1}{2}}\boldsymbol{G}_{mt}(\boldsymbol{I}_{n_T})^{\frac{1}{2}} \\
&= \frac{1}{\sqrt{m}}\boldsymbol{G}_{rm}(\boldsymbol{J}_m)^{\frac{1}{2}}\boldsymbol{G}_{mt} \\
&= \frac{1}{m}\boldsymbol{G}_{rm}\boldsymbol{J}_m\boldsymbol{G}_{mt} \\
&= \frac{1}{m}\begin{bmatrix}
(g_{rm_{1,1}}+\ldots+g_{rm_{1,m}})(g_{mt_{1,1}}+\ldots+g_{mt_{m,1}}) & \ldots & (g_{rm_{1,1}}+\ldots+g_{rm_{1,m}})(g_{mt_{1,n_T}}+\ldots+g_{mt_{m,n_T}}) \\
\vdots & \ddots & \vdots \\
(g_{rm_{n_R,1}}+\ldots+g_{rm_{n_R,m}})(g_{mt_{1,1}}+\ldots+g_{mt_{m,1}}) & \ldots & (g_{rm_{n_R,1}}+\ldots+g_{rm_{n_R,m}})(g_{mt_{1,n_t}}+\ldots+g_{mt_{m,n_t}})
\end{bmatrix}
\end{aligned}
$$

which is of the form

$$
\begin{bmatrix}
a_1b_1 & a_1b_2 & \ldots & a_1b_{n_T} \\
a_2b_1 & a_2b_2 & \ldots & a_2b_{n_T} \\
\vdots & \vdots & \ddots & \vdots \\
a_{n_R}b_1 & a_{n_R}b_2 & \ldots & a_{n_R}b_{n_T}
\end{bmatrix}.
$$

It was shown in Section 5.1.3 that such a matrix is rank 1. The elements g_{ij} of $\boldsymbol{G}_{rm}\boldsymbol{J}_m\boldsymbol{G}_{mt}$, which are given by

$$g_{ij} = (g_{rm_{i,1}} + \ldots + g_{rm_{i,m}})(g_{mt_{1,j}} + \ldots + g_{mt_{m,j}})$$

are distributed as $\mathcal{CN}(0, m^2)$, and the factor $\frac{1}{m}$ scales the distribution of the channel matrix entries to $\mathcal{CN}(0,1)$, yielding the desired normalized total channel energy of $||\boldsymbol{H}||_F^2 = n_R\, n_T$.

5.2.3 The Effect of Full Receive Antenna, Transmit Antenna, and Propagating Mode Decorrelation on the Gesbert Model Channel Matrix

Consider the situation where the receive antennas, transmit antennas and propagating modes are fully uncorrelated, $\boldsymbol{C}_r = \boldsymbol{I}_{n_R}, \boldsymbol{C}_t = \boldsymbol{I}_{n_T}$, and $\boldsymbol{C}_m = \boldsymbol{I}_m$. Substituting these values into (5.2) we get

$$
\begin{aligned}
\boldsymbol{H} &= \frac{1}{\sqrt{m}}(\boldsymbol{I}_{n_R})^{\frac{1}{2}}\boldsymbol{G}_{rm}(\boldsymbol{I}_m)^{\frac{1}{2}}\boldsymbol{G}_{mt}(\boldsymbol{I}_{n_T})^{\frac{1}{2}} \\
&= \frac{1}{\sqrt{m}}\boldsymbol{G}_{rm}\boldsymbol{G}_{mt} \\
&= \frac{1}{\sqrt{m}}\begin{bmatrix} g_{rm_{1,1}} & g_{rm_{1,2}} & \cdots & g_{rm_{1,m}} \\ g_{rm_{2,1}} & g_{rm_{2,2}} & \cdots & g_{rm_{2,m}} \\ \vdots & \vdots & \ddots & \vdots \\ g_{rm_{n_R,1}} & g_{rm_{n_R,2}} & \cdots & g_{rm_{n_R,m}} \end{bmatrix}\begin{bmatrix} g_{mt_{1,1}} & g_{mt_{1,2}} & \cdots & g_{mt_{1,n_T}} \\ g_{mt_{2,1}} & g_{mt_{2,2}} & \cdots & g_{mt_{2,n_T}} \\ \vdots & \vdots & \ddots & \vdots \\ g_{mt_{m,1}} & g_{mt_{m,2}} & \cdots & g_{mt_{m,n_T}} \end{bmatrix} \\
&= \frac{1}{\sqrt{m}}\begin{bmatrix} g_{rm_{1,1}}g_{mt_{1,1}} + \ldots + g_{rm_{1,m}}g_{mt_{m,1}} & \cdots \\ \vdots & \ddots \\ & g_{rm_{n_R,1}}g_{mt_{1,n_T}} + \ldots + g_{rm_{n_R,m}}g_{mt_{m,n_T}} \end{bmatrix} \\
&= \frac{1}{\sqrt{m}}\begin{bmatrix} g_{11} & g_{12} & \cdots & g_{1n_T} \\ \vdots & \vdots & \ddots & \vdots \\ g_{n_R1} & g_{n_R2} & \cdots & g_{n_Rn_T} \end{bmatrix}.
\end{aligned}
$$

The channel matrix is thus full rank. The matrix elements g_{ij}, which are given by

$$g_{ij} = g_{rm_{i,1}}g_{mt_{1,j}} + \ldots + g_{rm_{i,m}}g_{mt_{m,j}}$$

are distributed as $\mathcal{CN}(0, m)$, and the factor $1/\sqrt{m}$ scales the distribution of the channel matrix entries to $\mathcal{CN}(0, 1)$, yielding the desired normalized total channel energy of $||\boldsymbol{H}||_F^2 = n_R\, n_T$.

5.2.4 Summary

To summarize, the following observations can be made about the Gesbert model channel matrix:

- The presence of either full receive antenna correlation, full transmit antenna correlation, or full mode correlation will yield a rank 1 channel matrix.

- If receive antennas, transmit antennas and modes are fully uncorrelated, the channel matrix is given by a product of two Rayleigh distributed matrices, which can be represented as a single matrix with complex Gaussian entries. The channel matrix is full rank in this case.

- If receive and transmit antennas are fully uncorrelated, and modes are fully correlated, the channel matrix entries are given by a product of two iid complex Gaussian variables, and channel matrix rank is 1. Therefore the model supports the situation seen in Section 5.1.3 where the channel matrix entries are uncorrelated yet channel matrix rank is 1.

- If receive and transmit antennas are fully uncorrelated, the distribution of channel matrix entries will change smoothly from complex Gaussian, giving a full rank matrix, to a product of two iid complex Gaussian variables, giving a rank 1 matrix, as mode correlation is increased.

- The scaling factor $1/\sqrt{m}$ causes total channel energy to remain constant, regardless of the number of modes present.

The Gesbert model (5.2) yields channel matrices with the same rank properties as the channel matrices given by the HF MIMO channel matrix model (5.1), as antenna and mode correlation is varied. This means that measuring antenna correlation and mode correlation matrices, and using these matrices to generate a channel matrix, is a possible alternative to measuring the channel matrix directly, for the purposes of capacity calculations. The advantage of such an approach is that the system required to record data for calculation of correlation matrices is significantly less complex compared to the system required to record the channel matrix directly. Therefore, this is the approach that has been selected for the HF MIMO capacity investigation. The approach to calculating HF MIMO capacity is described in more detail in the next chapter.